

TOWARDS UNDERSTANDING THE ROBUSTNESS OF DIFFUSION-BASED PURIFICATION: A STOCHASTIC PERSPECTIVE

Anonymous authors

Paper under double-blind review

ABSTRACT

Diffusion-Based Purification (DBP) has emerged as an effective defense mechanism against adversarial attacks. The efficacy of DBP has been attributed to the forward diffusion process, which narrows the distribution gap between clean and adversarial images through the addition of Gaussian noise. Although this explanation has some theoretical support, the significance of its contribution to robustness remains unclear. In this paper, we argue that the inherent stochasticity in the DBP process is the primary driver of its robustness. To explore this, we introduce a novel Deterministic White-Box (DW-box) evaluation protocol to assess robustness in the absence of stochasticity and to analyze the attack trajectories and loss landscapes. Our findings suggest that DBP models primarily leverage stochasticity to evade effective attack directions, and their ability to purify adversarial perturbations can be weak. To further enhance the robustness of DBP models, we introduce Adversarial Denoising Diffusion Training (ADDT), which incorporates classifier-guided adversarial perturbations into diffusion training, thereby strengthening the DBP models' ability to purify adversarial perturbations. Additionally, we propose Rank-Based Gaussian Mapping (RBGM) to make perturbations more compatible with diffusion models. Experimental results validate the effectiveness of ADDT. In conclusion, our study suggests that future research on DBP can benefit from the perspective of decoupling the stochasticity-based and purification-based robustness.

1 INTRODUCTION

Deep learning has achieved remarkable success in various domains, including computer vision (He et al., 2016), natural language processing (OpenAI, 2023), and speech recognition (Radford et al., 2022). However, in this flourishing landscape, the persistent specter of adversarial attacks casts a shadow over the reliability of these neural models. Adversarial attacks for a vision model involve injecting imperceptible perturbations into input images to trick models into producing false outputs with high confidence (Goodfellow et al., 2015; Szegedy et al., 2014). This inspires a large amount of research on adversarial defense (Zhang et al., 2019; Samangouei et al., 2018; Shafahi et al., 2019; Wang et al., 2023).

Diffusion-based purification (DBP) (Nie et al., 2022) has recently gained recognition as a powerful defense mechanism against a range of adversarial attacks. Existing literature suggests that the robustness provided by DBP is primarily due to the forward diffusion process that narrows the distribution gap between clean and adversarial images through the application of Gaussian noise (Nie et al., 2022; Wang et al., 2022). However, although the reduction of the distribution gap is theoretically proven, its contribution to DBP robustness has not been sufficiently validated by empirical studies. Meanwhile, it is observed that the stochasticity of DBP may also contribute to the robustness (Nie et al., 2022).

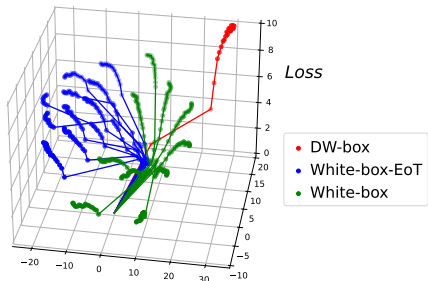


Figure 1: Comparison of attack trajectories under different evaluation settings. The attack trajectory in the standard White-box setting deviates significantly from the DW-box trajectory and shows lower effectiveness.

054 In light of this, we introduce an alternative perspective that highlights the role of stochasticity
055 throughout the DBP process as a key contributor to its robustness, challenging the traditional focus
056 on the forward diffusion process. To evaluate the impact of stochasticity, we employ a Deterministic
057 White-box (DW-box) attack setting where the attacker has complete knowledge of both the model
058 parameters and the stochastic elements. Our findings reveal that DBP models significantly lose their
059 robustness when the process is entirely deterministic to the attacker, thereby emphasizing the critical
060 importance of stochasticity. Further investigations into attack trajectories and the loss landscape
061 demonstrate that DBP models do not counter adversarial perturbations by a flat loss landscape as
062 adversarial training (AT) (Madry et al., 2018); instead, they rely on stochasticity to circumvent the
063 most effective attack direction, as depicted in Figure 1.

064 Building on our new perspective regarding DBP robustness, we hypothesize that it can be further
065 enhanced by improving the capability of the diffusion model to purify adversarial perturbations.
066 To test this hypothesis, we propose Adversarial Denoising Diffusion Training (ADDT) for DBP
067 models. This method follows an iterative two-step process: first, the Classifier-Guided Perturbation
068 Optimization (CGPO) step generates adversarial perturbations; then, the diffusion model training
069 step updates the parameters of the diffusion model using these perturbations. To better integrate these
070 perturbations within the diffusion framework, we introduce Rank-Based Gaussian Mapping (RBGM),
071 which adjusts the adversarial perturbations to more closely resemble Gaussian noise, in alignment with
072 the theory behind diffusion models. Experiments across various diffusion methods, attack settings,
073 and datasets suggest that ADDT can consistently enhance DBP models’ robustness and purification
074 ability. With further empirical analysis and discussions, we argue that future research on DBP should
075 decouple the robustness based on stochasticity and that achieved by purification, which suggests
076 two orthogonal directions for improving DBP: (1) enhancing its capability to purify adversarial
077 perturbations with efficient training methods, and (2) defending Expectation of Transformation (EoT)
078 attacks by increasing the variance of attack gradients.

078 Our main contributions are as follows:

- 080 • We present a novel perspective on DBP robustness, emphasizing the critical role of stochasticity and challenging the conventional purification-based belief that robustness primarily stems from reducing the distribution gap via the forward diffusion process.
- 083 • We introduce a new Deterministic White-box attack scenario and show that DBP models depend on stochastic attack gradients to avoid the most effective attack directions, demonstrating distinct properties compared to robust models obtained by adversarial training.
- 087 • Based on the proposed ADDT, we validate that the DBP robustness can be further enhanced by improving the capability of the diffusion model to purify adversarial perturbations.

090 2 RELATED WORK

092 **Adversarial training (AT).** First introduced by Madry et al. (2018), AT seeks to develop a robust classifier by incorporating adversarial examples into the training process. It has nearly become the de facto standard for enhancing the adversarial robustness of neural networks (Gowal et al., 2020; Rebuffi et al., 2021; Athalye et al., 2018). Recent advances in AT harness the generative power of diffusion models to augment training data and prevent AT from overfitting (Gowal et al., 2021; Wang et al., 2023). However, the application of AT to DBP methods has not been thoroughly explored.

099 **Adversarial purification.** Adversarial purification utilizes generative models to remove adversarial perturbation from inputs before they are processed by downstream models. Traditionally, generative adversarial networks (GANs) (Samangouei et al., 2018) or autoregressive models (Song et al., 2018) are employed as the purifier model. More recently, diffusion models have been introduced for adversarial purification, in a technique termed diffusion-based purification (DBP), and have shown promising results (Song & Ermon, 2019; Ho et al., 2020; Song et al., 2020a; Nie et al., 2022; Wang et al., 2022; Wu et al., 2022; Xiao et al., 2022). The robustness of DBP models is often attributed to the wash-out effect of Gaussian noise introduced during the forward diffusion process. Nie et al. (2022) propose that the forward process results in a reduction of the Kullback-Leibler (KL) divergence between the distributions of clean and adversarial images. Gao et al. (2022) suggest that while the forward diffusion process improves robustness by reducing model invariance, the backward process

restores this invariance, thereby undermining robustness. However, these theories explaining the robustness of DBP models lack substantial experimental support.

3 PRELIMINARIES

Adversarial training. Adversarial training aims to build a robust model by including adversarial samples during training (Madry et al., 2018). This approach can be formulated as a min-max problem, where it first generates adversarial samples (the maximization) and then adjusts the parameters to resist these adversarial samples (the minimization). Formally, this can be represented as:

$$\min_{\theta} \mathbb{E}_{(\mathbf{x}, y) \sim \mathcal{D}} [\max_{\delta \in B} L(f(\theta, \mathbf{x} + \delta), y)], \quad (1)$$

where L is the loss function, f is the classifier, $(\mathbf{x}, y) \sim \mathcal{D}$ denotes sampling training data from distribution \mathcal{D} , and B defines the set of permissible perturbation δ .

Diffusion models. Denoising Diffusion Probabilistic Models (DDPM) (Ho et al., 2020) and Denoising Diffusion Implicit Models (DDIM) (Song et al., 2020a) simulate a gradual transformation in which noise is added to images and then removed to restore the original image. The forward process can be represented as:

$$\mathbf{x}_t = \sqrt{\bar{\alpha}_t} \mathbf{x}_0 + \sqrt{1 - \bar{\alpha}_t} \boldsymbol{\epsilon}, \quad \boldsymbol{\epsilon} \sim \mathcal{N}(0, \mathbf{I}), \quad (2)$$

where \mathbf{x}_0 is the original image and \mathbf{x}_t is the noisy image. $\bar{\alpha}_t$ is the cumulative noise level at step t ($1 < t \leq T$, where T is the number of diffusion training steps). The model optimizes the parameters θ by minimizing the distance between the actual and predicted noise:

$$\theta^* = \arg \min_{\theta} \mathbb{E}_{\mathbf{x}_0, t, \boldsymbol{\epsilon}} [\|\boldsymbol{\epsilon} - \boldsymbol{\epsilon}_{\theta}(\sqrt{\bar{\alpha}_t} \mathbf{x}_0 + \sqrt{1 - \bar{\alpha}_t} \boldsymbol{\epsilon}, t)\|_2^2], \quad (3)$$

where $\boldsymbol{\epsilon}_{\theta}$ is the model’s noise prediction, with $\boldsymbol{\epsilon}_{\theta}$, we can predict $\hat{\mathbf{x}}_0$ in a single step:

$$\hat{\mathbf{x}}_0 = (\mathbf{x}_t - \sqrt{1 - \bar{\alpha}_t} \boldsymbol{\epsilon}_{\theta}(\mathbf{x}_t, t)) / \sqrt{\bar{\alpha}_t}, \quad (4)$$

where $\hat{\mathbf{x}}_0$ is the recovered image. DDPM typically takes an iterative approach to restore the image, removing a small amount of Gaussian noise at a time:

$$\hat{\mathbf{x}}_{t-1} = \left(\mathbf{x}_t - \frac{\beta_t}{\sqrt{1 - \bar{\alpha}_t}} \boldsymbol{\epsilon}_{\theta}(\mathbf{x}_t, t) \right) / \sqrt{1 - \beta_t} + \sqrt{\beta_t} \boldsymbol{\epsilon}, \quad (5)$$

where β_t is the noise level at step t , $\hat{\mathbf{x}}_{t-1}$ is the recovered image in step $t - 1$, $\boldsymbol{\epsilon}$ is sampled from $\mathcal{N}(0, \mathbf{I})$. DDIM proposes to speed up the denoising process by skipping certain intermediate steps. Recent work suggests that DDPM may also benefit from a similar approach (Nichol & Dhariwal, 2021). Score SDEs (Song et al., 2020b) give a score function view of DDPM and further lead to the derivations of DDPM++ (VPSDE) and EDM (Karras et al., 2022). In this diffusion process, the noise terms $\boldsymbol{\epsilon}$ in Equation (2) and Equation (5) represent the key stochastic elements that govern the randomness of the process. These stochastic elements will be further elaborated in Appendix C.1.

Diffusion-based purification (DBP). DBP uses diffusion models to remove adversarial perturbation from images. Instead of using a complete diffusion process between the clean image and pure Gaussian noise (between $t = 0$ and $t = T$), they first diffuse \mathbf{x}_0 to a predefined timestep $t = t^*$ ($t^* < T$) via Equation (2), and recover the image $\hat{\mathbf{x}}_0$ via the reverse diffusion process in Equation (5).

4 STOCHASTICITY-DRIVEN ROBUSTNESS OF DBP

4.1 STOCHASTICITY AS THE MAIN FACTOR OF DBP ROBUSTNESS

As discussed in Section 2, previous studies primarily attribute the robustness of DBP to the forward diffusion process, which introduces Gaussian noise to both clean and adversarial images, thereby narrowing the distribution gap between them (Wang et al., 2022; Nie et al., 2022). As a result, adversarial perturbation can be “washed out” by Gaussian noise. However, it is also found that the robustness of DiffPure can be reduced by switching the SDE sampling to ODE, which introduces less randomness, implying the potential contribution of stochasticity to DBP robustness (Nie et al., 2022).

To assess whether stochasticity has a significant influence on DBP robustness, we implement DDPM and DDIM within the DiffPure framework (Nie et al., 2022), resulting in $\mathbf{DP}_{\text{DDPM}}$ and $\mathbf{DP}_{\text{DDIM}}$.

162 respectively. Note that the original implementation of DiffPure adopts a DDPM discretization form
 163 of DDPM++ (VPSDE), which has minimal differences compared to DDPM. Therefore, the main
 164 difference between DiffPure and our DP_{DDPM} is that DiffPure employs a larger UNet. DDIM, which
 165 builds upon DDPM, introduces a deterministic ODE-based reverse process. DP_{DDPM} introduces
 166 Gaussian noise in both the forward and reverse processes, making the entire process stochastic. In
 167 contrast, DP_{DDIM} introduces Gaussian noise only in the forward process, and the reverse process
 168 is deterministic. The clean and robust accuracy of the two models on CIFAR-10 (Madry, 2017;
 169 Krizhevsky et al., 2009) under white-box PGD+EoT (Athalye et al., 2018) attack (as detailed in
 170 Section 6.1) are presented in Figure 2 (Clean and White). Although DP_{DDPM} achieves higher clean
 171 accuracy, it exhibits lower robust accuracy under adaptive white-box attacks, consistent with the
 172 observation by Nie et al. (2022). However, this comparison is insufficient to reveal the full role of
 173 stochasticity in DBP robustness, as the forward process of both DDPM and DDIM are stochastic.

174 To isolate the impact of stochasticity, we intro-
 175 duce a new attack scenario called the **Deterministic White-Box** (DW-box) setting. In this set-
 176 ting, the attacker has full knowledge of not only
 177 the model parameters but also the specific sam-
 178 pled values for the stochastic elements used dur-
 179 ing evaluation, effectively rendering the diffusion
 180 process deterministic from the attacker’s perspec-
 181 tive. This setting can be realistic if the attacker is
 182 aware of the seed or initial random state for the
 183 pseudo-random number generation utilized by the
 184 model. Concretely, we define three levels of at-
 185 tacker knowledge for our evaluations: (1) the con-
 186 ventional **White-box** setting, where the attacker
 187 has access to the model parameters but not the
 188 stochastic elements; (2) **DW_{Fwd}-box/DW_{Rev}-box**
 189 setting, where the attacker knows the stochastic el-
 190 ements in the forward/reverse process, in addition
 191 to the model parameters; (3) **DW_{Both}-box** setting, where the attacker has full knowledge of the model
 192 parameters and all the stochastic elements in both the forward and reverse processes. Details of these
 193 settings are provided in Appendix C.2.

194 We evaluated adversarial robustness on CIFAR-10 using l_∞ attacks (see Section 6.1). Traditional
 195 theories emphasize forward diffusion as the primary defense mechanism, suggesting that both
 196 DP_{DDPM} and DP_{DDIM} should behave similarly under the DW_{Fwd} -box setting. However, if stochasticity
 197 throughout the diffusion process is crucial, DP_{DDIM} , which becomes deterministic under the DW_{Fwd} -
 198 box setting, should experience a notable reduction in robustness, similar to DP_{DDPM} in the DW_{Both} -
 199 box setting. As shown in Figure 2, in the DW_{Fwd} -box setting, DP_{DDPM} maintains a significant portion of
 200 its robustness, whereas DP_{DDIM} loses almost all of its resistance to adversarial attacks. Furthermore,
 201 DP_{DDPM} exhibits a substantial drop in robustness only when the attacker has full access to both
 202 the forward and reverse stochastic elements, as seen in the DW_{Both} -box setting. This suggests
 203 that stochasticity across both the forward and reverse diffusion processes plays a critical role in
 204 maintaining robustness, challenging the conventional focus on forward diffusion alone.

205 Our findings suggest that DBP models primarily use stochasticity to resist adversarial attacks, rather
 206 than mainly depending on forward diffusion to mitigate adversarial perturbations, and it also reveals
 207 that DBP itself lacks the ability to *effectively purify adversarial perturbations*.

208 4.2 EXPLAINING STOCHASTICITY-DRIVEN ROBUSTNESS

209 To elucidate the robustness of DBP models, partic-
 210 ularly under EoT evaluations, we analyze the per-
 211 formance of several DBP models—DiffPure, GDMP,
 212 DP_{DDPM} , and DP_{DDIM} —under white-box attacks with
 213 and without Expectation over Transformation (EoT)
 214 iterations (denoted as EoT10 and EoT1, respectively).
 215 The results shown in Table 1 suggest that these DBP
 models remain robust under white-box attacks, with

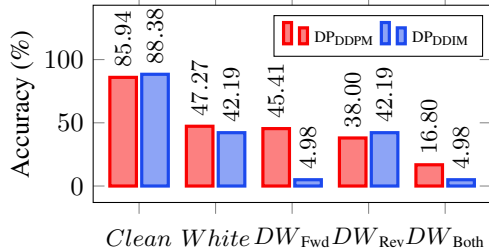


Figure 2: DP_{DDPM} and DP_{DDIM} robust accuracy under different attack settings on CIFAR-10. Both models lose most of their robustness only when the attacker knows all stochastic elements (DW_{Both} -box for DP_{DDPM} and DW_{Fwd} -box for DP_{DDIM}).

Table 1: Evaluation of state-of-the-art DBP methods, EoT significantly influences the evaluation accuracy (%) of model robustness.

	DiffPure	GDMP (MSE)	DP_{DDPM}	DP_{DDIM}
Clean	89.26	91.80	85.94	88.38
PGD20-EoT1	69.04	53.13	60.25	54.59
PGD20-EoT10	55.96	40.97	47.27	42.19

EoT evaluations resulting in moderate reductions in robustness. The detailed discussion on the selection of PGD and EoT steps is provided in Appendix E and Appendix A.

To gain deeper insights, we visualize the attack trajectories using t-SNE, projecting them onto an xy -plane with loss values represented along the z -axis. We compare trajectories for three types of attacks: white-box without EoT (White-box), white-box with EoT (White-box-EoT), and Deterministic White-box (DW-box). As shown in Figure 1, the trajectories exhibit high variance across all settings, reflecting the stochastic nature of DBP models. Specifically, DW-box attacks lead to a significant increase in loss values, whereas white-box attacks, even with EoT, result in only moderate increases. This suggests that *stochasticity prevents attackers from finding the optimal attack direction*. Specifically, due to the significant variance of the attack gradients, even if the EoT direction is an accurate estimation of the mean gradient direction, it may not be completely consistent with the most effective direction corresponding to the DW-box attack, thus resulting in a decline in attack performance. Additional evidences are provided in Appendix B.

Further analysis of the loss landscape, presented in Figure 3, illustrates key differences between White-box-EoT and Deterministic White-box attacks. The trajectory of the White-box-EoT attack diverges from the Deterministic White-box direction, resulting in a flatter loss landscape along the White-box-EoT path. This behavior indicates that White-box-EoT attacks fail to identify the most effective direction due to the stochastic nature of DBP models. In contrast, the Deterministic White-box attack induces a sharp increase in loss, revealing that when stochasticity is removed, the model becomes more vulnerable to adversarial perturbations. These findings differ from models trained using AT, where the whole loss landscape tends to remain flat and resistant across adversarial directions (Shafahi et al., 2019).

To conclude, it is suggested that instead of *possessing a flat loss landscape*, DBP models rely on stochasticity to *evade the most effective attack directions*. Note that while certified defense methods like random smoothing also incorporate stochasticity (Xiao et al., 2022; Carlini et al., 2022), their mechanisms and implications differ from those of DBP methods, as discussed in Appendix D.

5 TOWARDS IMPROVING THE PURIFICATION CAPABILITY OF DBP

Based on the analysis from Section 4, although the stochasticity-driven robustness of DBP does not depend on the flatness of the loss landscape, flattening the landscape can still benefit the DBP robustness given the non-trivial loss increment along the EoT direction. To achieve a flat loss landscape, we need to introduce adversarial samples to the training of the DBP models and minimize the loss on them. From the perspective of adversarial purification, this amounts to improving the diffusion model in its ability to purify adversarial perturbations.

To this end, we propose **Adversarial Denoising Diffusion Training (ADDT)**, which integrates adversarial perturbations into the training of the diffusion model in DBP. ADDT employs an iterative two-step procedure: (1) **Classifier-Guided Perturbation Optimization (CGPO)**, which generates adversarial perturbations by maximizing the classification error of a pre-trained classifier; (2) **Diffusion Model Training**, which updates the diffusion model using these perturbations to improve its capability of adversarial purification.

Integrating adversarial perturbations into diffusion training poses a challenge due to the Gaussian noise assumption inherent in diffusion models. To address this, we introduce **Rank-Based Gaussian Mapping (RBGM)**, a technique designed to transform adversarial perturbations into a form consistent with the Gaussian noise assumption. RBGM renders the perturbations more “Gaussian-like”, facilitating their integration into the diffusion training process.

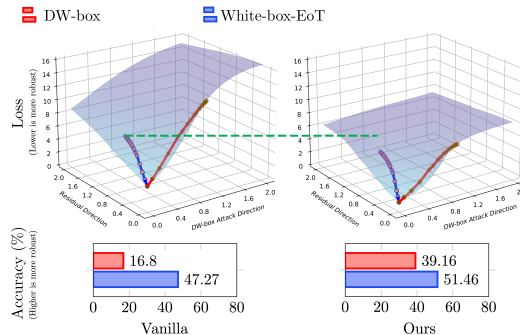


Figure 3: Visualisation of attack trajectories for White-box-EoT attacks and DW-box attacks on the loss landscape. The loss landscape is steep in the direction of the DW-box attack. The plot is based on the first 128 images of CIFAR-10.

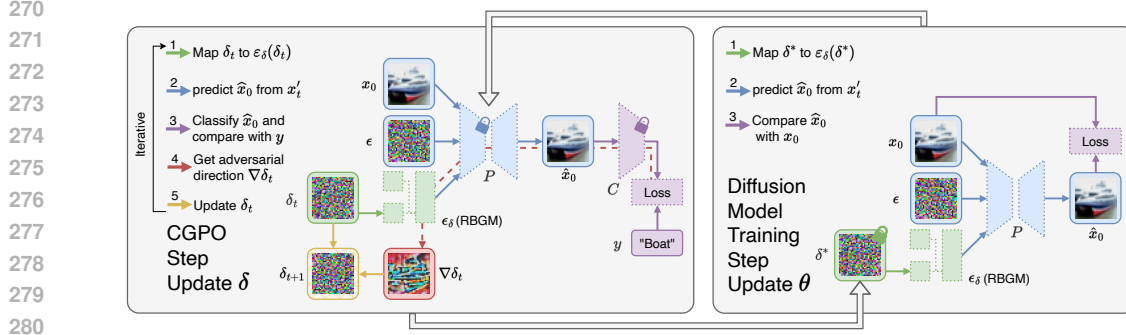


Figure 4: Overview of Adversarial Denoising Diffusion Training (ADDT). ADDT alternates between a CGPO step (left grey box) to refine the perturbations with a frozen diffusion model and classifier, and a training step (right grey box) to update the diffusion model with the refined perturbation. Throughout the process, RBGM is used to make the perturbation more “Gaussian-like”.

An overview of ADDT is illustrated in Figure 4, with pseudocode in Appendix G. The following subsections detail the components of ADDT.

5.1 ADVERSARIAL DENOISING DIFFUSION TRAINING

Classifier-Guided Perturbation Optimization (CGPO) step. In this step, we aim to refine adversarial perturbations δ in a way that maximizes the classification error of a pre-trained classifier C . The process starts by reconstructing a clean image \hat{x}_0 from the perturbed input x'_t using the diffusion model P . $P(\theta, x'_t, t)$ denotes a one-step diffusion process, which takes the noisy input x'_t and time step t and reconstructs the image \hat{x}_0 , following the formulation in Equation (4). The classifier C is then applied to this reconstructed image \hat{x}_0 to predict a label. To maximize the prediction error compared to the true label y , the optimization objective for refining δ can be defined as:

$$\delta^* = \arg \max_{\delta} \mathbb{E}_{x_0, t, \epsilon} [L(C(P(\theta, x'_t(x_0, \epsilon, \epsilon_{\delta}(\delta)), t)), y)], \quad (6)$$

where $L(\cdot, y)$ denotes the loss function used to measure the discrepancy between the classifier’s predicted label and the true label y . During the optimization, since RBGM is non-differentiable, we accumulate the gradient $\epsilon_{\delta}(\delta)$ to δ . Notably, the classifier in this process serves purely for semantic guidance and does not have to be consistent with the protected model. Further discussions on cross-classifier performance are provided in Section 6.2.

Diffusion Model Training step. The goal of this step is to update the diffusion model parameters to accurately recover the original image x_0 from a perturbed version x'_t . As depicted on the right side of Figure 4, The model is optimized to subtract both the Gaussian noise and the RBGM-mapped adversarial perturbations, effectively denoising the input. The optimization objective is defined as:

$$\theta^* = \arg \min_{\theta} \mathbb{E}_{x_0, t, \epsilon} \left[\frac{\sqrt{\bar{\alpha}_t}}{\sqrt{1 - \bar{\alpha}_t}} \|x_0 - P(\theta, x'_t, t)\|_2^2 \right], \quad (7)$$

where the expectation is taken over the distribution of original images $x_0 \sim \mathcal{D}$, time steps $t \sim \mathcal{U}(\{1, \dots, T\})$, and Gaussian noise $\epsilon \sim \mathcal{N}(0, \mathbf{I})$. The perturbed input x'_t is formed from the original image x_0 , Gaussian noise ϵ , and the RBGM-mapped adversarial perturbation $\epsilon_{\delta}(\delta)$, as defined in Equation (8). The scaling factor $\sqrt{\bar{\alpha}_t}/\sqrt{1 - \bar{\alpha}_t}$ ensures consistency with the standard formulation of DDPM/DDIM loss. This factor reflects the expected squared error between the noise introduced to the input and the noise removed by the diffusion model during denoising.

5.2 RANK-BASED GAUSSIAN MAPPING

Traditional diffusion models operate under the premise that input images are corrupted by independent Gaussian noise ϵ . To ensure that the perturbations remain Gaussian-like while capturing adversarial characteristics, we introduce the Rank-Based Gaussian Mapping (RBGM), illustrated in Figure 5.

Table 2: Clean and robust accuracy (%) on CIFAR-10 obtained by different DBP methods. All methods show consistent improvement fine-tuned with ADDT.

Diffusion model	DBP model	Clean	l_∞	l_2
-	-	95.12	0.00	1.46
DDIM	DP _{DDIM}	88.38	42.19	70.02
	DP_{DDIM}+ADDT	88.77	46.48	71.19
DDPM	GDMP (No Guided) (Wang et al., 2022)	91.41	40.82	69.63
	GDMP (MSE) (Wang et al., 2022)	91.80	40.97	70.02
	GDMP (SSIM) (Wang et al., 2022)	92.19	38.18	68.95
	DP _{DDPM}	85.94	47.27	69.34
	DP_{DDPM}+ADDT	85.64	51.46	70.12
DDPM++	COUP (Zhang et al., 2024)	90.33	50.78	71.19
	DiffPure	89.26	55.96	75.78
	DiffPure+ADDT	89.94	62.11	76.66
EDM	DP _{EDM} (Appendix I)	86.43	62.50	76.86
	DP_{EDM}+ADDT (Appendix I)	86.33	66.41	79.16

Table 3: Clean and robust accuracy (%) on DP_{DDPM}. ADDT improve robustness across different NFEs, especially at lower NFEs (*: default DDPM generation setting; -: classifier only).

Dataset	NFEs	Vanilla			ADDT		
		Clean	l_∞	l_2	Clean	l_∞	l_2
CIFAR-10	-	95.12	0.00	1.46	95.12	0.00	1.46
	5	49.51	21.78	36.13	59.96	30.27	41.99
	10	73.34	36.72	55.47	78.91	43.07	62.97
	20	81.45	45.21	65.23	83.89	48.44	69.82
	50	85.54	46.78	68.85	85.45	50.20	69.04
	100*	85.94	47.27	69.34	85.64	51.46	70.12
CIFAR-100	-	76.66	0.00	2.44	76.66	0.00	2.44
	5	17.29	3.71	9.28	21.78	6.25	13.77
	10	34.08	10.55	19.24	40.62	14.55	27.25
	20	48.05	17.68	30.66	53.32	18.65	36.13
	50	55.57	20.02	37.70	59.47	22.75	40.72
	100*	57.52	20.41	37.89	59.18	23.73	41.70

The RBGM function, denoted by $\epsilon_\delta(\delta)$, takes a perturbation δ as input. The key idea is to preserve the rank ordering of the elements in δ but replace their actual values with those from a standard Gaussian distribution. Specifically, we sample a Gaussian tensor ϵ_s of the same dimensions as δ . We then sort the elements of both δ and ϵ_s respectively in ascending order. By mapping the sorted elements of δ to the corresponding elements of ϵ_s , we obtain $\epsilon_\delta(\delta)$, which approximates Gaussian-distributed but retains the structural information of δ . To further enhance the Gaussian nature of the noise, we mix the RBGM-mapped perturbation with additional random Gaussian noise.

By combining the RBGM-induced perturbation with Gaussian noise, we generate an adversarial input x'_t as follows:

$$x'_t(x_0, \epsilon, \epsilon_\delta(\delta)) = \sqrt{\alpha_t}x_0 + \sqrt{1 - \lambda_t^2}\sqrt{1 - \alpha_t}\epsilon + \lambda_t\sqrt{1 - \alpha_t}\epsilon_\delta(\delta), \quad (8)$$

where λ_t modulates the level of adversarial perturbation. This ensures that the overall noise remains largely independent of x_0 and that the perturbations do not overwhelm the denoising model’s learning capabilities. We determine λ_t using the following formulation:

$$\lambda_t = \text{clip}(\gamma_t\lambda_{unit}, \lambda_{min}, \lambda_{max}), \quad \gamma_t = \frac{\sqrt{\alpha_t}}{\sqrt{1 - \alpha_t}}, \quad (9)$$

where the `clip` function limits λ_t between λ_{min} and λ_{max} . **Additional details and discussions about RBGM can be found in Appendix K.**

6 EXPERIMENTS AND DISCUSSIONS

6.1 EXPERIMENT SETUPS

Classifier. We train a WideResNet-28-10 for 200 epochs following the methods in (Yoon et al., 2021; Wang et al., 2022), achieving 95.12% accuracy on CIFAR-10 and 76.66% on CIFAR-100 dataset.

DBP timestep. For the diffusion forward process, we adopt the same timestep settings as DiffPure (Nie et al., 2022). In continuous-time models, such as the VPSDE (DDPM++) variant, with the forward time parameter $0 \leq t \leq 1$, we set $t^* = 0.1$, which strikes a balance between noise introduction and computational efficiency. For discrete-time models, such as DDPM and DDIM, where $t = 0, 1, \dots, T$, we similarly set the timestep to $t^* = 0.1 \times T$. Additional settings and results on DP_{EDM} are provided in Appendix I.

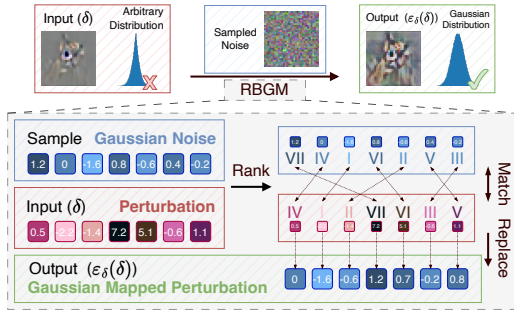


Figure 5: Rank-Based Gaussian Mapping. RBGM trims the input to follow Gaussian distribution. It samples a Gaussian noise and then replaces elements in the input with those from the Gaussian noise, matched according to their respective ranks.

Robustness evaluation. We employ PGD20+EoT10 (Athalye et al., 2018) for assessing model robustness. For ℓ_∞ -norm attacks, we set the step size $\alpha = 2/255$ and the maximum perturbation $\epsilon = 8/255$, while for ℓ_2 -norm attacks, we use $\alpha = 0.1$ and $\epsilon = 0.5$. Due to the high computational cost of EoT attacks, we evaluate our models on the first 1024 images for CIFAR-10 and CIFAR-100 datasets.

ADDT. ADDT fine-tuning is guided by the pre-trained WideResNet-28-10 classifier. For the CIFAR-10 dataset, we utilize the pre-trained exponential moving average (EMA) diffusion model from Ho et al. (2020), which has been converted into the Huggingface Diffusers format by Fang et al. (2023). For the CIFAR-100 dataset, we fine-tune this CIFAR-10 diffusion model over 100 epochs. In CGPO, we set the hyperparameters to $\lambda_{unit} = 0.03$, $\lambda_{min} = 0$, and $\lambda_{max} = 0.3$, and iteratively refine the perturbation δ for 5 steps. Additional details regarding computational cost are provided in Appendix P.

6.2 DEFENSE PERFORMANCE UNDER DIFFERENT CONDITIONS

Effectiveness of ADDT on different DBP models. We apply ADDT to a set of diffusion models and apply DiffPure-style DBP with the refined models. The comparison on clean and robust accuracy with the baseline and other DBP models is presented in Table 2. It shows that ADDT effectively enhances the robustness of these models.

Performance on different classifiers. We evaluate the cross-model protection ability of ADDT fine-tuned models by applying the diffusion model trained with WRN-28-10 guidance to other classifiers. The results in Table 4 indicate that the adversarial purification ability of these diffusion models could be transferred to different classifiers with various architectures. Notably, using a DP_{EDM} with WRN-28-10 Guidance training, we achieve 69.63% ℓ_∞ robust accuracy on a WRN-70-16 classifier. This demonstrates the feasibility of ADDT as it does not require classifier-specific fine-tuning.

Performance under acceleration. Speeding up the diffusion process by omitting intermediate steps has become a common practice in the use of diffusion models (Nichol & Dhariwal, 2021; Song et al., 2020a). Hence, we evaluate the robustness of accelerated DBP models. The computation cost is measured by the number of neural function evaluations (NFEs), which indicates the number of evaluation steps performed during the DBP backtracking process. For our experiments, we set $t^* = 0.1 \times T$ and accelerate the process by excluding intermediate time steps. For example, with 5 NFEs, the time steps for the DBP reverse process would be $t = [100, 80, 60, 40, 20, 0]$. The results in Table 3 validate the effectiveness of ADDT in improving the robustness of accelerated DP_{DDPM} models. Note that the performance of DP_{DDPM} varies significantly between different values of NFEs. This may be explained by the fact that DDPM introduces stochasticity (Gaussian noise) at each reverse step; with fewer reverse steps, its stochasticity reduces. Additionally, the generation capability of DDPM is sensitive to skipping of intermediate steps. We also conducted an evaluation of DP_{DDIM} models, as detailed in Appendix H.

6.3 ABLATION STUDY AND ANALYSIS

RBGM. We compare the generative ability of diffusion models fine-tuned from the same pre-trained

Table 4: Clean and robust accuracy (%) on CIFAR-10, obtained by different classifiers. ADDT (WRN-28-10 guidance) improves robustness in protecting different subsequent classifiers. (*: the classifier used in ADDT fine-tuning).

Model	Classifier	Vanilla			ADDT		
		Clean	ℓ_∞	ℓ_2	Clean	ℓ_∞	ℓ_2
DP _{DDPM-1000}	VGG-16 (Simonyan & Zisserman, 2014)	84.77	41.99	66.89	85.06	46.09	67.87
	ResNet-50 (He et al., 2016)	83.11	44.04	67.58	83.84	48.14	67.87
	WRN-28-10* (Zagoruyko & Komodakis, 2016)	85.94	47.27	69.34	85.64	51.46	70.12
	WRN-70-16 (Zagoruyko & Komodakis, 2016)	88.43	48.93	70.31	87.84	52.54	70.70
	ViT-B (Dosovitskiy et al., 2020)	85.45	45.61	69.53	85.25	48.63	69.92
DP _{DDIM-100}	VGG-16 (Simonyan & Zisserman, 2014)	87.16	29.00	61.82	87.55	35.06	66.11
	ResNet-50 (He et al., 2016)	86.04	31.74	62.11	86.57	38.77	65.82
	WRN-28-10* (Zagoruyko & Komodakis, 2016)	88.96	43.16	67.58	88.18	47.85	70.61
	WRN-70-16 (Zagoruyko & Komodakis, 2016)	84.40	39.16	68.36	84.96	47.66	69.14
	ViT-B (Dosovitskiy et al., 2020)	88.77	34.38	65.72	88.48	41.02	68.65
DP _{EDM}	WRN-28-10* (Zagoruyko & Komodakis, 2016)	86.43	62.50	76.86	86.33	66.41	79.16
	WRN-70-16 (Zagoruyko & Komodakis, 2016)	86.62	65.62	76.46	86.43	69.63	78.91

Table 5: Clean and robust accuracy (%) on CIFAR-10 fine-tuned with different training samples. (None: no fine-tuning)

Model	Training samples	Clean	ℓ_∞	ℓ_2
DDPM	None	85.94	47.27	69.34
	Clean	85.25	47.27	68.26
	MSE-guided	86.91	46.97	70.80
	CGPO	85.64	51.46	70.12
DDIM	None	88.96	43.16	67.58
	Clean	88.87	41.41	67.19
	MSE-guided	89.36	40.92	67.68
	CGPO	88.18	47.85	70.61

models using two different perturbations: RBGM-mapped perturbations and l_∞ perturbations. This evaluation is conducted by comparing their Fréchet Inception Distance (FID) scores (Heusel et al., 2017), as shown in Table 6. The results show that diffusion models fine-tuned with RBGM-mapped perturbations maintain generation quality comparable to the vanilla diffusion model, while models directly fine-tuned with l_∞ perturbations without RBGM show degraded performance. We also observe that training with RBGM-mapped perturbations generalized better to different attacks. Experimental details and additional tests are presented in Appendix M.

Table 6: FID score of DDPM for CIFAR-10 fine-tuned to different perturbations (the lower the better). Fine-tuning with RBGM-mapped perturbations yields lower FID scores than l_∞ perturbations (without RBGM).

	Vanilla	Clean Fine-tuning	ADDT	ADDT w/o RBGM
FID	3.196	3.500	5.190	13.608

CGPO. We analyze the effect of fine-tuning using different training samples in Table 5. Specifically, we compare the performance of samples generated with classifier guidance in the CGPO step, referred to as ‘‘CGPO’’, against those generated with Mean Squared Error (MSE) loss, noted as ‘‘MSE-guided’’. The evaluation results are presented for DDPM with 100 NFEs and DDIM with 10 NFEs. Results demonstrates that samples generated by CGPO significantly outperform MSE-guided samples in enhancing DBP robustness.

Revisiting DBP robustness. We re-examine robustness under the Deterministic White-box setting by comparing the performance of diffusion models with and without ADDT fine-tuning, as shown in Figure 6. The fine-tuned models show significantly higher robust accuracy under the DW-box setting, indicating improved non-stochasticity-based robustness brought by ADDT. Further experiments across different models and NFEs in Appendix N confirm these robustness improvements. We also compare the loss landscapes of ADDT fine-tuned models and vanilla diffusion models, as shown in Figure 3. This comparison shows that our method effectively smooths the loss landscape of DBP models and enhance its ability to purify adversarial perturbations. **Evaluation with stronger PGD+EoT attacks.** To balance computational cost and attack strength, we primarily employ the PGD20+EoT10 configuration in our evaluations. To further validate the efficacy of ADDT under stronger attack settings, we assess its performance using the more challenging PGD200+EoT20 setup. The results presented in Table 7 and Table 9 show that under these intensified attacks, ADDT’s robust accuracy experiences a moderate 5% drop compared to the PGD20+EoT10 setting. Nonetheless, across various settings and datasets, ADDT consistently demonstrates superior robust accuracy to the baseline.

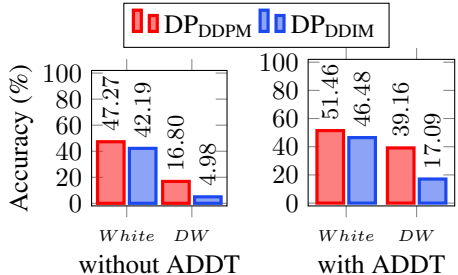


Figure 6: Revisiting robustness under Deterministic White-box setting. ADDT improves robustness under both White-box and Deterministic White-box setting, implying that ADDT strengthens the models’ ability to purify adversarial inputs.

6.4 SCALING TO MORE COMPLEX AND HIGH-DIMENSIONAL DATA

To evaluate the scalability of DBP and ADDT on more complex and high-dimensional datasets, we extend our experiments to include Tiny-ImageNet (Le & Yang, 2015) and ImageNet-1k (Deng et al., 2009). For Tiny-ImageNet, we trained the diffusion model from scratch for 200 epochs, followed by fine-tuning with ADDT for an additional 50 epochs, guided by a pretrained WRN-28-10 classifier. For ImageNet-1k, the diffusion model was trained from scratch for 12 epochs and then fine-tuned with ADDT for 8 epochs, using a pretrained ResNet-101 classifier as guidance.

Table 7: Robust accuracy (%) on CIFAR-10 under more PGD and EoT iterations.

Model	PGD200+EoT20		PGD20+EoT10	
	Vanilla (l_∞)	ADDT (l_∞)	Vanilla (l_∞)	ADDT (l_∞)
DP _{DDPM}	41.02	46.19	47.27	51.46
DP _{DDIM}	36.23	41.11	43.16	47.85
DiffPure	48.93	55.76	55.96	62.11

As shown in Table 8 and Table 9, ADDT successfully enhances the robustness of DBP on these complex datasets, while the improvement may be limited. Similar to the characteristics of adversarial training on classifiers, effective up-scaling of ADDT may require sufficient model capacity and a

Table 8: Clean and robust accuracy (%) on Tiny-ImageNet with WRN-28-10 classifier. ADDT improves DBP robustness on Tiny-ImageNet (-: classifier only).

Model	Vanilla			ADDT		
	Clean	l_∞	l_2	Clean	l_∞	l_2
-	71.37	0.00	0.00	-	-	-
DP _{DDPM-1000}	57.13	11.82	46.68	56.15	13.57	48.54
DP _{DDIM-100}	60.35	4.79	39.75	60.45	5.86	40.82
DP _{EDM}	57.03	19.14	46.00	56.45	20.61	47.95

Table 9: Clean and robust accuracy (%) on ImageNet-1k with ResNet-101 classifier. All experiments are conducted under l_∞ perturbation bound of $\epsilon = 4/255$.

Metric	Vanilla	ADDT
Clean Accuracy	80.31	80.20
PGD20+EoT10	46.92	48.02
PGD200+EoT20	35.31	35.83

large amount of data, and our results in Table 2 have demonstrated the benefits of applying a larger diffusion model in DBP. However, efficient training methods specialized for DBP models can be a promising direction for future studies.

In addition, we observe that the strong EoT attacks on images of higher resolution are computationally intensive. Specifically, our evaluation with PGD200+EoT20 on 1024 images of the size 224×224 requires approximately 7 days on 8 NVIDIA RTX 4090 GPUs. Therefore, we argue that the up-scaling in data dimension can also imply significantly increased computational costs for the attacker.

6.5 DISCUSSIONS ON IMPROVING STOCHASTICITY-BASED DBP ROBUSTNESS

As analyzed in Section 4.2, the DBP robustness can be primarily attributed to the high variance of the stochastic attack gradients. We argue that *increasing the variance of attack gradients* can improve the stochasticity-based robustness of DBP models by reducing the effectiveness of EoT attacks. Specifically, on the one hand, higher variance means higher errors in the estimation of the expected attack gradient direction with a fixed number of samples, and to reduce the error, more EoT steps are required. On the other hand, higher variance also suggests that the expected deviation of the DW-box attack gradient (which suggests the most effective attack direction) deviates more from the EoT attack gradient, even if the estimation of the mean attack gradient is accurate. As discussed in Section 4.2, such deviation leads to lower increase in classification loss for one attack step, suggesting that a successful attack may not be achieved or require more PGD steps.

To increase the variance of attack gradients, an intuitive approach is to introduce more stochasticity. As an initial experiment, we augment the DBP framework’s stochasticity by integrating a *Corrector sampler*. Specifically, Song et al. (2021) develop a Predictor-Corrector (PC) sampler framework. While standard VPSDE (DDPM++) implementations typically use only the predictor component, we add a Corrector sampler to increase stochasticity in the reverse diffusion process, thereby boosting the overall variance of attack gradients. As detailed in Appendix J, our preliminary results indicate that this modification improves the robustness of DBP models against adaptive White-box attacks. However, there is a trade-off: the model’s clean accuracy decreases slightly. These observations align with the findings of Nie et al. (2022), where randomizing the diffusion timesteps also leads to robustness improvements at the cost of clean accuracy, as well as with prior research on stochastic preprocessing defenses (Gao et al., 2022).

7 CONCLUSION

This study offers a new perspective on the robustness of Diffusion-Based Purification (DBP), emphasizing the crucial role of stochasticity and challenging the traditional view that robustness is mainly derived from minimizing the distribution gap through the forward diffusion process. We introduce a Deterministic white-box (DW-box) attack scenario and show that DBP models are based on stochastic elements to evade effective attack directions and lack the ability to purify adversarial perturbations, demonstrating distinct properties compared to models trained with Adversarial Training. To further enhance the robustness of DBP models, we develop Adversarial Denoising Diffusion Training (ADDT) and Rank-Based Gaussian Mapping (RBGM). ADDT integrates adversarial perturbations into the training process, while RBGM trims perturbations to more closely resemble Gaussian distributions. Experiments across various diffusion methods, attack settings, and datasets suggest the effectiveness of ADDT. In summary, this study highlights the decoupling of stochasticity-based and purification-based robustness of DBP models for deeper analysis, and suggests combining them for better robustness in practice.

REFERENCES

- 540
541
542 Anish Athalye, Nicholas Carlini, and David Wagner. Obfuscated gradients give a false sense of
543 security: Circumventing defenses to adversarial examples. In *International conference on machine*
544 *learning*, pp. 274–283. PMLR, 2018.
- 545 Nicholas Carlini, Florian Tramer, Krishnamurthy Dvijotham, Leslie Rice, Mingjie Sun, and J Zico
546 Kolter. (certified!!) adversarial robustness for free! In *The Eleventh International Conference on*
547 *Learning Representations*, 2022.
- 548 Huanran Chen, Yinpeng Dong, Zhengyi Wang, Xiao Yang, Chengqi Duan, Hang Su, and Jun Zhu.
549 Robust classification via a single diffusion model. *arXiv preprint arXiv:2305.15241*, 2023.
- 550
551 Tianqi Chen, Bing Xu, Chiyuan Zhang, and Carlos Guestrin. Training deep nets with sublinear
552 memory cost. *arXiv preprint arXiv:1604.06174*, 2016.
- 553
554 Jeremy Cohen, Elan Rosenfeld, and Zico Kolter. Certified adversarial robustness via randomized
555 smoothing. In *international conference on machine learning*, pp. 1310–1320. PMLR, 2019.
- 556 Francesco Croce and Matthias Hein. Reliable evaluation of adversarial robustness with an ensemble
557 of diverse parameter-free attacks. In *International conference on machine learning*, pp. 2206–2216.
558 PMLR, 2020.
- 559 Francesco Croce, Maksym Andriushchenko, Vikash Sehwal, Edoardo Debenedetti, Nicolas Flam-
560 marion, Mung Chiang, Prateek Mittal, and Matthias Hein. Robustbench: a standardized adversarial
561 robustness benchmark. *arXiv preprint arXiv:2010.09670*, 2020.
- 562
563 Jia Deng, Wei Dong, Richard Socher, Li-Jia Li, Kai Li, and Li Fei-Fei. Imagenet: A large-scale
564 hierarchical image database. In *2009 IEEE conference on computer vision and pattern recognition*,
565 pp. 248–255. Ieee, 2009.
- 566 Alexey Dosovitskiy, Lucas Beyer, Alexander Kolesnikov, Dirk Weissenborn, Xiaohua Zhai, Thomas
567 Unterthiner, Mostafa Dehghani, Matthias Minderer, Georg Heigold, Sylvain Gelly, et al. An
568 image is worth 16x16 words: Transformers for image recognition at scale. *arXiv preprint*
569 *arXiv:2010.11929*, 2020.
- 570
571 Gongfan Fang, Xinyin Ma, and Xinchao Wang. Structural pruning for diffusion models. *arXiv*
572 *preprint arXiv:2305.10924*, 2023.
- 573
574 Yue Gao, Ilia Shumailov, Kassem Fawaz, and Nicolas Papernot. On the limitations of stochastic
575 pre-processing defenses. *Advances in Neural Information Processing Systems*, 35:24280–24294,
576 2022.
- 577 Ian J. Goodfellow, Jonathon Shlens, and Christian Szegedy. Explaining and harnessing adversarial
578 examples. In Yoshua Bengio and Yann LeCun (eds.), *3rd International Conference on Learning*
579 *Representations, ICLR 2015, San Diego, CA, USA, May 7-9, 2015, Conference Track Proceedings*,
580 2015. URL <http://arxiv.org/abs/1412.6572>.
- 581
582 Sven Gowal, Chongli Qin, Jonathan Uesato, Timothy A. Mann, and Pushmeet Kohli. Uncovering the
583 limits of adversarial training against norm-bounded adversarial examples. *CoRR*, abs/2010.03593,
584 2020. URL <https://arxiv.org/abs/2010.03593>.
- 585 Sven Gowal, Sylvestre-Alvise Rebuffi, Olivia Wiles, Florian Stimberg, Dan Andrei Calian, and
586 Timothy A Mann. Improving robustness using generated data. *Advances in Neural Information*
587 *Processing Systems*, 34:4218–4233, 2021.
- 588
589 Kaiming He, Xiangyu Zhang, Shaoqing Ren, and Jian Sun. Deep residual learning for image
590 recognition. In *Proceedings of the IEEE conference on computer vision and pattern recognition*,
591 pp. 770–778, 2016.
- 592 Martin Heusel, Hubert Ramsauer, Thomas Unterthiner, Bernhard Nessler, and Sepp Hochreiter. Gans
593 trained by a two time-scale update rule converge to a local nash equilibrium. *Advances in neural*
information processing systems, 30, 2017.

- 594 Jonathan Ho, Ajay Jain, and Pieter Abbeel. Denoising diffusion probabilistic models. *arXiv preprint*
595 *arxiv:2006.11239*, 2020.
- 596
- 597 Mintong Kang, Dawn Song, and Bo Li. Diffattack: Evasion attacks against diffusion-based adversarial
598 purification. *Advances in Neural Information Processing Systems*, 36, 2024.
- 599 Tero Karras, Miika Aittala, Timo Aila, and Samuli Laine. Elucidating the design space of diffusion-
600 based generative models. *Advances in Neural Information Processing Systems*, 35:26565–26577,
601 2022.
- 602 Alex Krizhevsky, Geoffrey Hinton, et al. Learning multiple layers of features from tiny images. 2009.
- 603
- 604 Ya Le and Xuan Yang. Tiny imagenet visual recognition challenge. *CS 231N*, 7(7):3, 2015.
- 605
- 606 Aleksander Madry. Towards deep learning models resistant to adversarial attacks. *arXiv preprint*
607 *arXiv:1706.06083*, 2017.
- 608 Aleksander Madry, Aleksandar Makelov, Ludwig Schmidt, Dimitris Tsipras, and Adrian Vladu.
609 Towards deep learning models resistant to adversarial attacks. In *6th International Conference on*
610 *Learning Representations, ICLR 2018, Vancouver, BC, Canada, April 30 - May 3, 2018, Conference*
611 *Track Proceedings*. OpenReview.net, 2018. URL <https://openreview.net/forum?id=rJzIBfZAb>.
- 612
- 613 Alexander Quinn Nichol and Prafulla Dhariwal. Improved denoising diffusion probabilistic models.
614 In *International Conference on Machine Learning*, pp. 8162–8171. PMLR, 2021.
- 615
- 616 Weili Nie, Brandon Guo, Yujia Huang, Chaowei Xiao, Arash Vahdat, and Anima Anandkumar.
617 Diffusion models for adversarial purification. In *International Conference on Machine Learning*
618 *(ICML)*, 2022.
- 619 OpenAI. Gpt-4 technical report. *ArXiv*, abs/2303.08774, 2023. URL [https://api.](https://api.semanticscholar.org/CorpusID:257532815)
620 [semanticscholar.org/CorpusID:257532815](https://api.semanticscholar.org/CorpusID:257532815).
- 621
- 622 Alec Radford, Jong Wook Kim, Tao Xu, Greg Brockman, Christine McLeavey, and Ilya Sutskever.
623 Robust speech recognition via large-scale weak supervision. *ArXiv*, abs/2212.04356, 2022. URL
624 <https://api.semanticscholar.org/CorpusID:252923993>.
- 625 Sylvestre-Alvise Rebuffi, Sven Gowal, Dan Andrei Calian, Florian Stimberg, Olivia Wiles, and Timo-
626 thy A. Mann. Fixing data augmentation to improve adversarial robustness. *ArXiv*, abs/2103.01946,
627 2021. URL <https://api.semanticscholar.org/CorpusID:232092181>.
- 628
- 629 Pouya Samangouei, Maya Kabkab, and Rama Chellappa. Defense-gan: Protecting classifiers against
630 adversarial attacks using generative models. *arXiv preprint arXiv:1805.06605*, 2018.
- 631 Ali Shafahi, Mahyar Najibi, Mohammad Amin Ghiasi, Zheng Xu, John Dickerson, Christoph Studer,
632 Larry S Davis, Gavin Taylor, and Tom Goldstein. Adversarial training for free! *Advances in*
633 *Neural Information Processing Systems*, 32, 2019.
- 634 Karen Simonyan and Andrew Zisserman. Very deep convolutional networks for large-scale image
635 recognition. *arXiv preprint arXiv:1409.1556*, 2014.
- 636
- 637 Jiaming Song, Chenlin Meng, and Stefano Ermon. Denoising diffusion implicit models.
638 *arXiv:2010.02502*, October 2020a. URL <https://arxiv.org/abs/2010.02502>.
- 639 Yang Song and Stefano Ermon. Generative modeling by estimating gradients of the data distribution.
640 *Advances in neural information processing systems*, 32, 2019.
- 641
- 642 Yang Song, Taesup Kim, Sebastian Nowozin, Stefano Ermon, and Nate Kushman. Pixeldefend:
643 Leveraging generative models to understand and defend against adversarial examples. In *Inter-*
644 *national Conference on Learning Representations*, 2018. URL [https://openreview.net/](https://openreview.net/forum?id=rJUYGxbCW)
645 [forum?id=rJUYGxbCW](https://openreview.net/forum?id=rJUYGxbCW).
- 646 Yang Song, Jascha Sohl-Dickstein, Diederik P Kingma, Abhishek Kumar, Stefano Ermon, and Ben
647 Poole. Score-based generative modeling through stochastic differential equations. *arXiv preprint*
arXiv:2011.13456, 2020b.

- 648 Yang Song, Jascha Sohl-Dickstein, Diederik P Kingma, Abhishek Kumar, Stefano Ermon, and Ben
649 Poole. Score-based generative modeling through stochastic differential equations. In *International
650 Conference on Learning Representations*, 2021. URL [https://openreview.net/forum?
651 id=PXTIG12RRHS](https://openreview.net/forum?id=PXTIG12RRHS).
- 652 Christian Szegedy, Wojciech Zaremba, Ilya Sutskever, Joan Bruna, Dumitru Erhan, Ian J. Goodfellow,
653 and Rob Fergus. Intriguing properties of neural networks. In Yoshua Bengio and Yann LeCun
654 (eds.), *2nd International Conference on Learning Representations, ICLR 2014, Banff, AB, Canada,
655 April 14-16, 2014, Conference Track Proceedings*, 2014. URL [http://arxiv.org/abs/
656 1312.6199](http://arxiv.org/abs/1312.6199).
- 657 Jinyi Wang, Zhaoyang Lyu, Dahua Lin, Bo Dai, and Hongfei Fu. Guided diffusion model for
658 adversarial purification. *arXiv preprint arXiv:2205.14969*, 2022.
- 660 Zekai Wang, Tianyu Pang, Chao Du, Min Lin, Weiwei Liu, and Shuicheng Yan. Better diffusion
661 models further improve adversarial training. In *International Conference on Machine Learning
662 (ICML)*, 2023.
- 663 Quanlin Wu, Hang Ye, and Yuntian Gu. Guided diffusion model for adversarial purification from
664 random noise. *arXiv preprint arXiv:2206.10875*, 2022.
- 666 Chaowei Xiao, Zhongzhu Chen, Kun Jin, Jiongxiao Wang, Weili Nie, Mingyan Liu, Anima Anand-
667 kumar, Bo Li, and Dawn Song. Densepure: Understanding diffusion models towards adversarial
668 robustness. *arXiv preprint arXiv:2211.00322*, 2022.
- 669 Jongmin Yoon, Sung Ju Hwang, and Juho Lee. Adversarial purification with score-based generative
670 models. In *International Conference on Machine Learning*, pp. 12062–12072. PMLR, 2021.
- 672 Sergey Zagoruyko and Nikos Komodakis. Wide residual networks. *arXiv preprint arXiv:1605.07146*,
673 2016.
- 674 Hongyang Zhang, Yaodong Yu, Jiantao Jiao, Eric Xing, Laurent El Ghaoui, and Michael Jordan.
675 Theoretically principled trade-off between robustness and accuracy. In *International conference on
676 machine learning*, pp. 7472–7482. PMLR, 2019.
- 677 Mingkun Zhang, Jianing Li, Wei Chen, Jiafeng Guo, and Xueqi Cheng. Classifier guidance enhances
678 diffusion-based adversarial purification by preserving predictive information, 2024. URL [https:
679 //openreview.net/forum?id=qvLPtx52ZR](https://openreview.net/forum?id=qvLPtx52ZR).
- 680
681
682
683
684
685
686
687
688
689
690
691
692
693
694
695
696
697
698
699
700
701

A INFLUENCE OF EoT ITERATIONS ON DBP ROBUSTNESS EVALUATION

In this section, we examine how the number of EoT iterations influences the DBP robustness evaluation. As previously discussed in Section 4.1, the Deterministic White-box attack could find the most effective attack direction. To quantify the impact of EoT iterations, we compare the attack direction of the standard White-box-EoT across various numbers of EoT iterations with that of the Deterministic White-box.

See Figure 7 for a visual explanation, where the red line shows the DBP accuracy after attack, and the blue line shows the similarity between the attack directions of the White-box-EoT and Deterministic White-box. The results show a clear trend: increasing the EoT iterations raises the similarity between the attack directions and reduces model accuracy. However, both the increase in similarity and the decline in accuracy decelerate with further iterations.

Balancing computational cost and evaluation accuracy, we chose the PGD20-EoT10 configuration for our robustness evaluation.

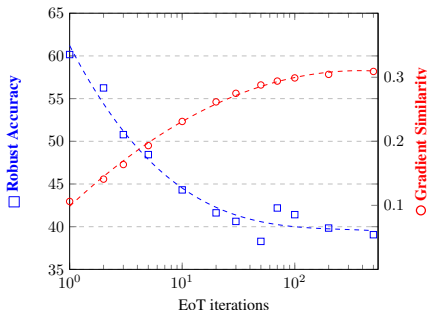


Figure 7: Robust accuracy (%) and gradient similarity on DP_{DDPM} for CIFAR-10, obtained by different EoT iterations. As the number of EoT iterations increases, the gradient similarity between the White-box-EoT attack direction and the Deterministic White-box attack direction increases and the robust accuracy decreases.

B DBP MODELS EMPLOYING DIFFERENT STOCHASTIC ELEMENTS CANNOT BE ATTACKED ALL AT ONCE

Previous research has questioned whether stochasticity can improve robustness, arguing that it can produce obfuscated gradients that give a false sense of security (Athalye et al., 2018). To investigate this, we implement $DW_{\text{semi-box}}$, a semi-stochastic setting that restricts the stochastic elements to a limited set of options. Our results show that stochasticity can indeed improve robustness, even when the attacker has full knowledge of all the possible options for stochastic elements.

Building on the concept of Deterministic White-box, we further propose $DW_{\text{semi-128}}$ to explore whether stochasticity can indeed improve robustness. Unlike under Deterministic White-box, where the attacker attacks a DBP model under the exact set of stochastic noise used in the evaluation, $DW_{\text{semi-128}}$ relaxes the stochastic elements to a limited set of options, the attacker should simultaneously attack over 128 different sets of stochastic noise. It uses the average adversarial direction from these 128 noise settings (EoT-128) to perturb the DBP model. To understand the impact of stochasticity, we analyze the changes of the model loss under DW-box attack and $DW_{\text{semi-128}}$ attack. We plot these changes by adjusting a factor k to modify an image x with a perturbation σ , evaluating the loss at $x + k\sigma$ where k varies from -16 to 16 . We generate perturbations with l_∞ Fast Gradient Sign Method (FGSM) (Goodfellow et al., 2015) with magnitude $1/255$. The plot is evaluated using WideResNet-28-10 with DP_{DDPM} over the first 128 images of CIFAR-10 dataset.

As Figure 8 shows, in the Deterministic White-box setting, the perturbations significantly increase the loss, proving their effectiveness. However, for $DW_{\text{semi-128}}$, where the attack spans multiple noise setting, the increase in loss is more moderate. This suggests that even when the attackers are fully informed about the stochastic noise choices, stochasticity still improves the robustness of the DBP.

756
757
758
759
760
761
762
763
764
765
766
767
768
769
770
771
772
773
774
775
776
777
778
779
780
781
782
783
784
785
786
787
788
789
790
791
792
793
794
795
796
797
798
799
800
801
802
803
804
805
806
807
808
809

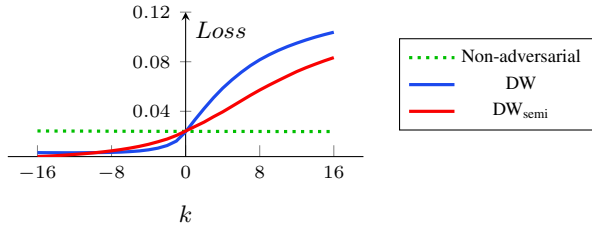


Figure 8: Impact of stochasticity on perturbation efficacy. Perturbations created under DW_{semi} -box setting are less potent compared to DW -box setting. For non-adversarial perturbations, we randomly assign each element a value of either $1/255$ or $-1/255$.

This challenges the notion that there exists a vulnerable direction that is effective for all stochastic noise.

C IMPACT OF ATTACKERS’ KNOWLEDGE ON ROBUSTNESS: COMPARISON OF ATTACK SETTINGS

This appendix delves into the influence of varying levels of attackers’ knowledge about the stochastic components in diffusion processes on the robustness of diffusion-based models. We specifically assess the individual contributions of the forward and reverse diffusion processes to model robustness across different attack scenarios.

C.1 STOCHASTIC ELEMENTS IN THE DIFFUSION PROCESSES

Unlike deterministic models, where outputs are solely determined by the inputs, diffusion models introduce stochastic elements that also influence the outcomes. To clarify the attacker’s knowledge, we first explain the stochastic components involved in diffusion processes.

In the **forward diffusion process**, Gaussian noise is incorporated into the input data to derive a noisy version x_t :

$$x_t = \sqrt{\alpha_t} x + \sqrt{1 - \alpha_t} \epsilon_f, \tag{10}$$

where $\epsilon_f \sim \mathcal{N}(0, I)$ is sampled once per input.

In the **reverse diffusion process**, the model progressively denoises x_t through iterative steps. For the Denoising Diffusion Probabilistic Model (DDPM), the reverse process is inherently stochastic:

$$x_{t-1} = \frac{1}{\sqrt{\alpha_t}} \left(x_t - \frac{1 - \alpha_t}{\sqrt{1 - \bar{\alpha}_t}} \epsilon_{\theta(x_t, t)} \right) + \sigma_t \epsilon_t, \tag{11}$$

where $\epsilon_t \sim \mathcal{N}(0, I)$ is sampled at each reverse step. In contrast, for the Denoising Diffusion Implicit Model (DDIM), the reverse process is deterministic, and no noise $\{\epsilon_t\}_{t=1}^T$ is added.

C.2 ATTACK SETTINGS AND ATTACKER KNOWLEDGE

We delineate four distinct attack scenarios, each characterized by the extent of information available to the attacker, particularly concerning the Gaussian noise variables in the diffusion process. Table 10 provides a summary of the attacker’s knowledge in each scenario.

In the conventional white-box attack setting, the attacker possesses comprehensive knowledge of the model architecture and parameters but lacks insight into the stochastic elements used during inference (ϵ_f and $\{\epsilon_t\}_{t=1}^T$). The DW_{Fwd} setting grants the attacker knowledge of the Gaussian noise in the forward diffusion process (ϵ_f). Conversely, the DW_{Rev} setting provides the attacker with knowledge of the Gaussian noise introduced during the reverse diffusion steps ($\{\epsilon_t\}_{t=1}^T$). The DW_{Both} setting offers the attacker complete access to all stochastic elements, ϵ_f and $\{\epsilon_t\}_{t=1}^T$. By manipulating the attacker’s knowledge in this manner, we isolate the individual effects of the forward and reverse diffusion processes on model robustness.

Table 10: Information accessible to the attacker in different attack settings. ϵ_f denotes the Gaussian noise in the forward process, and $\{\epsilon_t\}_{t=1}^T$ represents the Gaussian noise in the reverse process.

Attacker’s Knowledge	White-box	DW _{Fwd}	DW _{Rev}	DW _{Both}
Model Architecture and Parameters	✓	✓	✓	✓
Input Images and Class Labels	✓	✓	✓	✓
Forward Process Noise ϵ_f	×	✓	×	✓
Reverse Process Noise $\{\epsilon_t\}_{t=1}^T$	×	×	✓	✓

C.3 IMPLICATIONS OF THE ATTACKER’S KNOWLEDGE OF STOCHASTIC ELEMENTS

The attacker’s capability to craft potent adversarial examples is significantly influenced by their knowledge of the stochastic elements in diffusion processes. When these elements are unknown to the attacker, they must independently sample noise variables, leading to discrepancies between their approximations and the actual behavior of the victim model. Conversely, if the attacker is privy to the exact noise variables used during inference, they can precisely mimic the model’s behavior, markedly boosting the efficacy of their attack.

Attacker Without Knowledge of Stochastic Elements. In scenarios where the attacker lacks access to specific noise variables ϵ_f and $\{\epsilon_t\}_{t=1}^T$, the model’s output becomes unpredictable from the attacker’s viewpoint. The attacker must then optimize the expected value of the loss function over the distribution of these stochastic elements. The optimization problem for devising an adversarial example x^{adv} is formulated as:

$$x^{\text{adv}} = \arg \max_{\|x^{\text{adv}} - x\| \leq \delta} \mathbb{E}_{\epsilon_f, \{\epsilon_t\}} [\mathcal{L}(f(x^{\text{adv}}; \epsilon_f, \{\epsilon_t\}), y)], \tag{12}$$

where δ specifies the permissible perturbation magnitude, \mathcal{L} is the loss function, f represents the model’s output given the input and stochastic elements, and y is the actual class label.

Attacker With Knowledge of Stochastic Elements. Should the attacker possess exact knowledge of the noise variables ϵ_f and $\{\epsilon_t\}_{t=1}^T$ utilized during the model’s inference, they can accurately emulate the victim classifier’s behavior. The stochastic processes become deterministic from the attacker’s perspective, facilitating the formulation of the optimization problem as:

$$x^{\text{adv}} = \arg \max_{\|x^{\text{adv}} - x\| \leq \delta} \mathcal{L}(f(x^{\text{adv}}; \epsilon_f, \{\epsilon_t\}), y). \tag{13}$$

This precise knowledge allows the attacker to adopt the exact noise that will be used during the target evaluation, allowing effective evaluation.

C.4 EFFECT OF ATTACKER’S KNOWLEDGE ON MODEL ROBUSTNESS

We test the robustness of DDPM under these four settings, and Table 11 encapsulates the result.

Table 11: Robust accuracy (%) of DDPM under different attack settings.

Attack Setting	Robust Accuracy (l_∞)
Conventional White-Box Attack	47.27
DW _{Fwd}	45.41
DW _{Rev}	35.25
DW _{Both}	16.80

Conventional White-Box Attack. In this setting, the attacker fully understands the model’s architecture and parameters but lacks knowledge of the stochastic elements (ϵ_f and $\{\epsilon_t\}_{t=1}^T$) used

during inference. The model’s output remains unpredictable due to the stochasticity of both diffusion processes, making it challenging for the attacker to generate effective adversarial examples (reaching robust accuracy of **47.27%**).

DW_{Fwd}. Here, the attacker is aware of the Gaussian noise ϵ_f used in the forward diffusion process but not of the noise $\{\epsilon_t\}_{t=1}^T$ in the reverse process. This partial knowledge allows the attacker to accurately simulate the forward process, reducing uncertainty in this phase. However, the reverse process remains unpredictable. The slight decrease in robust accuracy to **45.41%** suggests that while forward process stochasticity contributes to robustness, its effect is somewhat diminished when compromised.

DW_{Rev}. In this scenario, the attacker knows the noise variables $\{\epsilon_t\}_{t=1}^T$ used in the reverse diffusion steps but not the forward process noise ϵ_f . This knowledge enables the attacker to align their strategy more closely with the actual behavior of the model during reverse diffusion, resulting in a more noticeable drop in robust accuracy to **35.25%**. The reverse process’s stochasticity appears to play a more critical role in model robustness compared to the forward process.

DW_{Both}. When the attacker has comprehensive knowledge of both the forward and reverse process noise variables, they can replicate both diffusion processes accurately, eliminating any stochasticity from their perspective. This complete predictability allows for precise adversarial example crafting, leading to a significant reduction in robust accuracy to **16.80%**. This demonstrates that the combined stochastic elements are crucial for maintaining robustness; when fully exposed, the model’s defense mechanisms are substantially weakened.

D THE ROLE OF STOCHASTICITY IN DBP COMPARED TO CERTIFIED DEFENSE METHODS

In this appendix section, we delve deeper into the role of randomness in Diffusion-Based Prediction (DBP) models and contrast it with its role in certified defense methods such as randomized smoothing (Cohen et al., 2019). While both approaches incorporate stochasticity, their mechanisms and implications for adversarial robustness differ significantly.

- Conventionally, the classification models discussed in the studies of adversarial robustness can be viewed as mappings from input space X to the label space Y . However, DBP additionally involves a random variable $\epsilon \in E$ that determines the random sampling in the forward and reverse processes (which can be the random seed in implementation). Hence, a DBP model f can be viewed as the mapping $f : (X, E) \rightarrow Y$.
- Previous studies on randomized smoothing treat the randomized model f as a mapping $f : X \rightarrow P_Y$, where P_Y is the space of label distribution. Typically, the final prediction can be formulated as $F(x) = \arg \max_c [f(x)]_c$, i.e., the class c with the highest probability in the output distribution $\mathbb{f}(x)$. Apparently, F deterministically maps X to Y , consistent with the conventional models.
- Recent studies on DBP also regard the model as $f : X \rightarrow P_Y$, without explicitly studying the role of ϵ . *The key difference between DBP and randomized smoothing is that the final prediction for an input x is directly sampled from the distribution $f(x)$ for once, instead of sampling multiple times to approximate $F(x)$ as in randomized smoothing.*
- In this paper, we revisit DBP by treating the randomized model f as the mapping $f : (X, E) \rightarrow Y$ and studying the role of $\epsilon \in E$ as an input of f . From this perspective, the conventional adversarial setting assuming full knowledge of the model parameters (but not ϵ) is not a complete white box, which motivates us to study the DW-box setting.
- From our perspective, we can clearly point out the difference between DBP and randomized smoothing in terms of the loss landscape. Given an input x_0 , the local loss landscape for a DBP model f is not deterministic as it also depends on ϵ . *Although the expected loss landscape over $\epsilon \in E$ may be smooth, it does not suggest the robustness of DBP, as ϵ is fixed during a single inference run of DBP.* Indeed, our study suggests that given x_0 and a fixed ϵ_0 , the local landscape of DBP is likely not smooth. In contrast, the loss landscape of a

randomized smoothing model F may be smooth as it is the average landscape over multiple ϵ . To conclude, we argue that the random noise itself may not smooth the loss landscape, but the average over random noises may.

E ATTACK METHOD AND SETTINGS

Previous assessments of DBP robustness have often utilized potentially unreliable methods. In particular, due to the iterative denoising process in diffusion models, some studies resort to mathematical approximations of gradients to reduce memory constraints (Athalye et al., 2018) or to circumvent the diffusion process during backpropagation (Wang et al., 2022). Furthermore, the reliability of AutoAttack, a widely used evaluation method, in assessing the robustness of DBP models is questionable. Although AutoAttack includes a *Rand* version designed for stochastic models, Nie et al. (2022) have found instances where the *Rand* version is less effective than the *Standard* version in evaluating DBP robustness.

To improve the robustness evaluation of diffusion-based purification (DBP) models, we implement several modifications. First, to ensure the accuracy of the gradient computations, we compute the exact gradient of the entire diffusion classification pipeline. To mitigate the high memory requirements in diffusion iterative denoising steps, we use gradient checkpointing (Chen et al., 2016) techniques to optimize memory usage. In addition, to deal with the stochastic nature of the DBP process, we incorporate the Expectation over Transformation (EoT) method to average gradients across different attacks. We adopt EoT with 10 iterations, and a detailed discussion of the choice of EoT iterations can be found in Appendix A. We also use the Projected Gradient Descent (PGD) attack instead of AutoAttack for our evaluations¹. Our revised robustness evaluation revealed that DBP models, such as DiffPure and GDMP, perform worse than originally claimed. DiffPure’s accuracy dropped from a claimed 70.64% to an actual 55.96%, and GDMP’s from 90.10% to 40.97%. These results emphasize the urgent need for more accurate and reliable evaluation methods to properly assess the robustness of DBP models. Similar evaluation protocols are also applied in Chen et al. (2023); Kang et al. (2024).

F EXPERIMENTAL SETTING OF VISUALIZATION OF THE ATTACK TRAJECTORY

We visualize the attack by plotting the loss landscape and trace the trajectories of EoT attack under White-box setting and the Deterministic White-box setting in Figure 3. We run a vanilla PGD20-EoT10 attack under White-box setting and a PGD20 attack under Deterministic White-box setting. We then expand a 2D space using the final perturbations from these two attacks, draw the loss landscape, and plot the attack trajectories on it. Note that the two adversarial perturbation directions are not strictly orthogonal. To extend this 2D space, we use the Deterministic White-box attack direction and the orthogonal component of the EoT attack direction. Note that the endpoints of both trajectories lie exactly on the loss landscape, while intermediate points are projected onto it. The plot is evaluated using WideResNet-28-10 with DP_{DDPM} over the first 128 images of CIFAR-10 dataset.

G PSEUDO-CODE OF ADDT

The pseudo-code for adopting ADDT within DDPM and DDIM framework is shown in Algorithm 1.

H ADDT RESULTS ON DP_{DDIM}

As shown in Table 12, the performance of DP_{DDIM} is less sensitive to the number of function evaluations (NFEs). Additionally, ADDT consistently improved the robustness of DP_{DDIM} .

¹We discover a bug in the *Rand* version of AutoAttack that causes it to overestimate the robustness of DBP. After fixing this, AutoAttack gives similar results to PGD attacks, but at a much higher computational cost. We discuss this in detail in Appendix L.

Algorithm 1 Adversarial Denoising Diffusion Training (ADDT)

Require: \mathbf{x}_0 is image from training dataset, y is the class label of the image, C is the classifier, \mathbf{P} is one-step diffusion reverse process and $\boldsymbol{\theta}$ is its parameter, L is CrossEntropy Loss.

```

1: for  $\mathbf{x}_0, y$  in the training dataset do
2:    $t \sim \text{Uniform}(\{1, \dots, T\})$ 
3:    $\lambda_t = \text{clip}(\gamma_t \lambda_{\text{unit}}, \lambda_{\min}, \lambda_{\max})$ , where  $\gamma_t = \frac{\sqrt{\bar{\alpha}_t}}{\sqrt{1-\bar{\alpha}_t}}$ 
4:   Init  $\boldsymbol{\delta}$  to a small random vector.
5:   for 1 to  $\text{ADDT}_{\text{iterations}}$  do
6:      $\boldsymbol{\epsilon} \sim \mathcal{N}(0, I)$ 
7:      $\boldsymbol{\epsilon}' = \text{RBGM}(\boldsymbol{\delta}, \boldsymbol{\epsilon})$ 
8:      $\mathbf{x}_t = \sqrt{\bar{\alpha}_t} \mathbf{x}_0 + \sqrt{1 - \lambda_t^2} \sqrt{1 - \bar{\alpha}_t} \boldsymbol{\epsilon} + \lambda_t \sqrt{1 - \bar{\alpha}_t} \boldsymbol{\epsilon}'$ 
9:      $\boldsymbol{\delta} = \boldsymbol{\delta} + \nabla_{\boldsymbol{\epsilon}'} L(C(\mathbf{P}(\mathbf{x}_t, t), y))$ 
10:  end for
11:   $\boldsymbol{\epsilon} \sim \mathcal{N}(0, I)$ 
12:   $\boldsymbol{\epsilon}' = \text{RBGM}(\boldsymbol{\delta}, \boldsymbol{\epsilon})$ 
13:   $\mathbf{x}_t = \sqrt{\bar{\alpha}_t} \mathbf{x}_0 + \sqrt{1 - \lambda_t^2} \sqrt{1 - \bar{\alpha}_t} \boldsymbol{\epsilon} + \lambda_t \sqrt{1 - \bar{\alpha}_t} \boldsymbol{\epsilon}'$ 
14:  Take a gradient descent step on:
     $\nabla_{\boldsymbol{\theta}} \left\| \frac{\sqrt{\bar{\alpha}_t}}{\sqrt{1-\bar{\alpha}_t}} (\mathbf{x}_0 - \mathbf{P}(\mathbf{x}_t, t)) \right\|_2^2$ 
15: end for
Diffusion model  $\boldsymbol{\epsilon}_{\boldsymbol{\theta}}$  predicts the Gaussian noise added to the image, adopting Equation (4) in the paper, we
have  $\mathbf{P}(\mathbf{x}_t, t) = (\mathbf{x}_t - \sqrt{1 - \bar{\alpha}_t} \boldsymbol{\epsilon}_{\boldsymbol{\theta}}(\mathbf{x}_t, t)) / \sqrt{\bar{\alpha}_t}$ 

```

Table 12: Clean and robust accuracy (%) on DP_{DDIM}. ADDT improve robustness across different NFEs (*: default DDIM generation setting, -: classifier only).

Dataset	NFEs	Vanilla			ADDT		
		Clean	l_{∞}	l_2	Clean	l_{∞}	l_2
CIFAR-10	-	95.12	0.00	1.46	95.12	0.00	1.46
	5	89.65	42.19	68.65	88.57	47.27	70.61
	10*	88.96	43.16	67.58	88.18	47.85	70.61
	20	87.89	41.70	69.24	88.67	48.63	69.73
	50	88.96	42.48	68.85	88.57	46.68	69.24
	100	88.38	42.19	70.02	88.77	46.48	71.19
CIFAR-100	-	76.66	0.00	2.44	76.66	0.00	2.44
	5	62.11	15.43	35.74	62.79	17.58	38.87
	10*	62.21	15.33	36.52	64.45	20.02	39.26
	20	63.67	15.62	37.89	65.23	18.65	40.62
	50	62.40	16.31	37.79	63.87	19.14	39.94
	100	63.28	15.23	36.62	66.02	18.85	39.84

I ADOPTING VPSDE(DDPM++) AND EDM MODELS IN DBP

In the previous discussion of the robustness of DBP models, as detailed in Section 4.1, our focus was primarily on the DDPM and DDIM models. We now extend our analysis to include VPSDE (DDPM++) and EDM (Karras et al., 2022) models. VPSDE (DDPM++) is the diffusion model used in DiffPure.

From a unified perspective, diffusion process can be modeled by stochastic differential equations (SDE) (Song et al., 2021). The forward SDE, as described in Equation (14), converts a complex initial data distribution into a simpler, predetermined prior distribution by progressively infusing noise. This can also be done in a single step, as shown in Equation (15), mirroring the strategy of DDPM described in Equation (2). Reverse SDE, as explained in Equation (16), reverses this process, restoring the noise distribution to the original data distribution, thus completing the diffusion cycle.

$$d\mathbf{x} = \mathbf{f}(\mathbf{x}, t)dt + g(t)d\mathbf{w}, \quad (14)$$

$$p_{0t}(\mathbf{x}(t) | \mathbf{x}(0)) = \mathcal{N}\left(\mathbf{x}(t); e^{-\frac{1}{4}t^2(\bar{\beta}_{\max} - \bar{\beta}_{\min}) - \frac{1}{2}t\bar{\beta}_{\min}} \mathbf{x}(0), \mathbf{I} - \mathbf{I}e^{-\frac{1}{2}t^2(\bar{\beta}_{\max} - \bar{\beta}_{\min}) - t\bar{\beta}_{\min}}\right), \quad t \in [0, 1] \quad (15)$$

$$d\bar{\mathbf{x}} = [\mathbf{f}(\mathbf{x}, t) - g^2(t)\nabla_{\mathbf{x}} \log p_t(\mathbf{x})] dt + g(t)d\bar{\mathbf{w}}. \quad (16)$$

The reverse process of SDEs also derives equivalent ODEs Equation (17) for fast sampling and exact likelihood computation, and this Score ODEs corresponds to DDIM.

$$d\mathbf{x} = \left[\mathbf{f}(\mathbf{x}, t) - \frac{1}{2}g(t)^2 \nabla_{\mathbf{x}} \log p_t(\mathbf{x}) \right] dt. \quad (17)$$

By modulating the stochasticity, we can craft a spectrum of semi-stochastic models that bridge pure SDEs and deterministic ODEs, offering a range of stochastic behaviors.

EDM provides a unified framework to synthesize the design principles of different diffusion models (DDPM, DDIM, iDDPM (Nichol & Dhariwal, 2021), VPSDE, VESDE (Song et al., 2021)). Within this framework, EDM incorporates efficient sampling methods, such as the Heun sampler, and introduces optimized scheduling functions $\sigma(t)$ and $s(t)$. This allows EDM to achieve state-of-the-art performance in generative tasks.

EDM forward process could be presented as:

$$\mathbf{x}_t = \mathbf{x}_0 + \sigma(t^*) * \boldsymbol{\epsilon}, \quad \boldsymbol{\epsilon} \sim \mathcal{N}(0, \mathbf{I}), \quad (18)$$

where we choose $\sigma(t^*) = 0.5$ for clean and robust accuracy tradeoff. And for reverse process, EDM incorporates a parameter S_{churn} to modulate the stochastic noise infused during the reverse process. For our experiments, we choose 50 reverse steps (50 NFEs, NFEs is Function of Neural Function Evaluations), configured the parameters with $S_{min} = 0.01$, $S_{max} = 0.46$, $S_{noise} = 1.007$, and designate $S_{churn} = 0$ to represent EDM-ODE, $S_{churn} = 6$ to represent EDM-SDE.

As shown in Table 13, our ADDT could also increase the robustness of DP_{EDM} .

Table 13: Clean and robust accuracy (%) on DP_{EDM} for CIFAR-10. ADDT improves robustness in both $DP_{EDM-SDE}$ and $DP_{EDM-ODE}$.

Type	Vanilla		ADDT	
	$DP_{EDM-SDE}$	$DP_{EDM-ODE}$	$DP_{EDM-SDE}$	$DP_{EDM-ODE}$
Clean	86.43	87.99	86.33	87.99
l_{∞}	62.50	60.45	66.41	64.16
l_2	76.86	75.49	79.16	77.15

J STRENGTHENING DBP VIA AUGMENTED STOCHASTICITY

Song *et al.* present a Predictor-Corrector sampler for SDEs reverse process for VPSDE (DDPM++) (as detailed in Appendix I of Song et al. (2021)). However, standard implementations of VPSDE (DDPM++) typically use only the Predictor. Given our hypothesis that stochasticity contributes to robustness, we expect that integrating the Corrector sampler into VPSDE (DDPM++) would further enhance the robustness of DBP models. Our empirical results, as shown in Table 14, confirm that the inclusion of a Corrector to VPSDE (DDPM++) indeed improve the model’s defenses ability against adversarial attacks with l_{∞} norm constraints. This finding supports our claim that the increased stochasticity can further strengthen DBP robustness. Adding Corrector is also consistent with ADDT. Note that the robustness against l_2 norm attacks does not show a significant improvement with the integration of the Extra Corrector. A plausible explanation for this could be that the robustness under l_2 attacks is already quite strong, and the compromised performance on clean data counteracts the increase in robustness.

Table 14: Clean and robust accuracy (%) on DP_{DDPM++} for CIFAR-10. Both extra Corrector and ADDT fine-tuning improved robustness.

Type	Vanilla	Extra Corrector	ADDT	ADDT+Extra Corrector
Clean	89.26	85.25	89.94	85.55
l_{∞}	55.96	59.77	62.11	65.23
l_2	75.78	74.22	76.66	76.66

K DISCUSSION ABOUT RBGM-MAPPED PERTURBATIONS

K.1 MOTIVATION AND ADVANTAGES OF RBGM

In Section 4, we discuss the limitations of Diffusion-Based Perturbation (DBP) models in effectively purifying adversarial perturbations. To overcome these limitations and simultaneously preserve the generative ability of the diffusion models, we introduce a novel approach: incorporating “adversarially selected Gaussian noise” into the diffusion training process.

To elaborate, a conventional diffusion forward process is based on the equation:

$$x_t = \sqrt{\bar{\alpha}_t} x_0 + \sqrt{1 - \bar{\alpha}_t} \epsilon, \quad (19)$$

where x_t represents the noisy image at time t , x_0 is the initial input, $\bar{\alpha}_t$ is a time-dependent scaling factor, and ϵ is random Gaussian noise. Our proposed method, ADDT, modifies this equation to include an adversarial component:

$$x_t = \sqrt{\bar{\alpha}_t} x_0 + \sqrt{1 - \lambda_t^2} \sqrt{1 - \bar{\alpha}_t} \epsilon + \lambda_t \sqrt{1 - \bar{\alpha}_t} \epsilon_\delta(\delta). \quad (20)$$

In this revised formulation, $\epsilon_\delta(\delta)$ represents the adversarial perturbation, and λ_t is a parameter that controls the blend between traditional and adversarial noise. The core objective of ADDT training is to *generate perturbations that emulate the characteristics of Gaussian noise in conventional diffusion training while incorporating adversarial disturbances*.

This introduces our Rank-Based Gaussian Mapping (RBGM) technique, which retains the relative ordering of perturbation magnitudes while adjusting the values to more closely resemble a Gaussian distribution. The advantages of RBGM are twofold:

Enhancing statistical consistency. Raw adversarial perturbation values often exhibit non-standard distributions, and RBGM serves to recalibrate these perturbations, aligning them more closely with a Gaussian distribution. To elaborate, rather than enforcing a multivariate Gaussian distribution for the entire perturbation, RBGM ensures that the distribution of individual perturbation values adheres to Gaussian characteristics.

The benefit of this transformation can be illustrated in Figure 9 and Figure 10. For a fair comparison, the perturbation values have been normalized. In Figure 9, the original perturbation values display a wide array of distributions across different images and time steps. After the mapping of RBGM, these values are transformed to exhibit a uniform Gaussian distribution.

In Figure 10, the raw perturbations show irregular and inconsistent behavior when mixed with Gaussian noise at varying ratios. However, after RBGM adjustment, the perturbations and the mixture exhibit consistent statistics with the pure Gaussian noise. The statistical consistency of the perturbation values may ease the training of the diffusion model and avoid significant deviation from the normal diffusion process.

Reducing image-specific dependence. In the training of diffusion models, the Gaussian noise is independent of specific images or time steps. This approach contrasts with the nature of adversarial perturbations, which are typically tailored to each input. RBGM mitigates this by introducing stochasticity into the construction of perturbations and merely preserving the ranks of the values of the image-dependent adversarial perturbations, thus reducing image-specific dependence. This characteristic further ensures the resemblance of ADDT to the diffusion training process and potentially mitigates the overfitting of training images.

K.2 RBGM-MAPPED PERTURBATIONS PRESERVE ADVERSARIAL CHARACTERISTICS

While RBGM-mapped perturbations are “selected from a Gaussian distribution”, their actual distribution deviates from a pure Gaussian distribution, and are adversarial for models. To substantiate this claim, we compare the influence of RBGM-mapped perturbations and Gaussian noise on model performance. In our experiments, we perturb clean images by adding RBGM-mapped perturbations

1134
1135
1136
1137
1138
1139
1140
1141
1142
1143
1144
1145
1146
1147
1148
1149
1150
1151
1152
1153
1154
1155
1156
1157
1158
1159
1160
1161
1162
1163
1164
1165
1166
1167
1168
1169
1170
1171
1172
1173
1174
1175
1176
1177
1178
1179
1180
1181
1182
1183
1184
1185
1186
1187

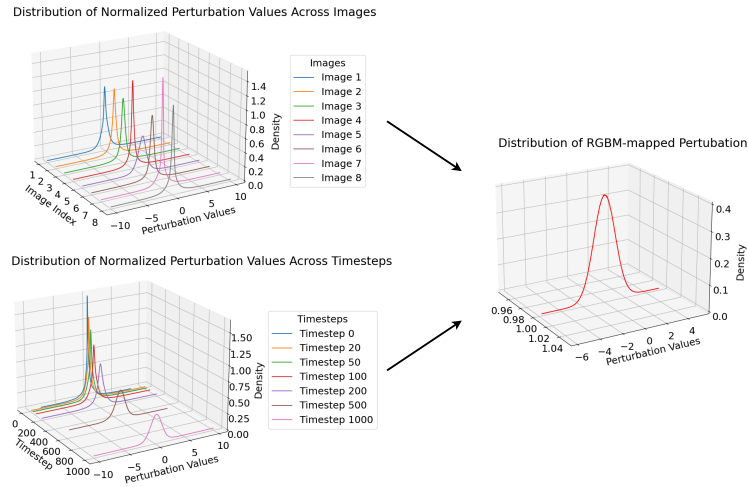


Figure 9: Raw perturbation values exhibit diverse distributions across images and time steps. RBGM maps these perturbations to a uniform Gaussian distribution.

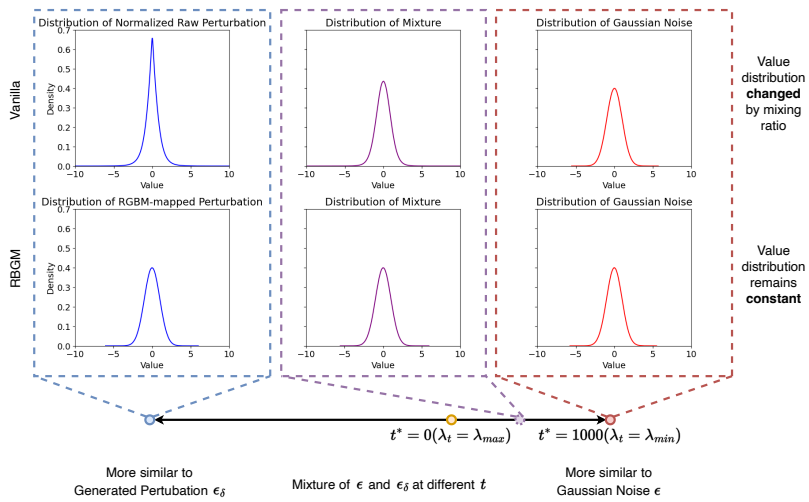


Figure 10: RBGM ensures that mixing perturbations with Gaussian noise at any ratio yields a consistent value distribution.

and Gaussian noise, each scaled by a factor of 0.03. The results present in Table 15 demonstrate that RBGM-mapped perturbations effectively act as adversarial inputs to the model. These perturbations drastically reduce the accuracy of a pre-trained clean WRN-28-10 from 95.12% to 4.47%.

Table 15: Comparison of model accuracy under different conditions. RBGM-mapped perturbations lead to a significant reduction in accuracy compared to Gaussian noise.

Model	Clean	Gaussian noise	RBGM-mapped perturbation
WRN-28-10	95.12	81.54	4.47

K.3 BLENDING ADVERSARIAL PERTURBATIONS INTO DIFFUSION MODEL TRAINING

In conventional adversarial attacks, perturbations are directly applied to the image, resulting in an adversarial image:

$$x_{\text{adv}} = x_0 + \delta,$$

where x_0 is the original input image, and δ is the adversarial perturbation. In ADDT, we incorporate this concept into the diffusion process, redefining the noisy image at time step t as:

$$x_t = \sqrt{\bar{\alpha}_t}(x_0 + \delta) + \sqrt{1 - \bar{\alpha}_t}\epsilon,$$

To enable the diffusion model to effectively purify adversarial perturbations during training, we reformulate the above equation by merging the perturbation δ with the noise ϵ . This results in:

$$x_t = \sqrt{\bar{\alpha}_t}x_0 + \sqrt{1 - \bar{\alpha}_t}(\epsilon + \gamma_t\delta),$$

where γ_t is a scaling factor defined as:

$$\gamma_t = \frac{\sqrt{\bar{\alpha}_t}}{\sqrt{1 - \bar{\alpha}_t}}.$$

Since $\bar{\alpha}_t$ is a time-dependent parameter that monotonically decreases from 1 to 0 during the diffusion process, γ_t spans the range from 0 to ∞ . To ensure the adversarial perturbation remains within a manageable intensity, we constrain its value to the range between λ_{\min} and λ_{\max} .

K.4 RBGM ENHANCES PERTURBATION COMPATIBILITY WITH DIFFUSION MODEL TRAINING

To illustrate how RBGM enhances the compatibility of perturbations with diffusion model training, we conduct comparative analyses in two scenarios. First, we assess the impact of RBGM on statistical consistency by comparing Gaussian noise with adversarial perturbations reordered based on Gaussian noise ranks. Second, we evaluate the effectiveness of RBGM-mapped perturbations in improving model robustness while maintaining generative performance by comparing them with ℓ_2 -normalized perturbations.

Gaussian noise vs. adversarial perturbations ordered by Gaussian noise We begin by examining RBGM’s influence on statistical consistency through two training methodologies:

1. **Vanilla:** Trained with standard Gaussian noise.
2. **ADDT_{Gaussian reordered}:** Trained with adversarial perturbations reordered according to Gaussian noise ranks. To ensure a fair comparison, the perturbations are normalized to have a mean of 0 and a variance of 1, as their original magnitudes (derived from accumulated gradients) are significantly smaller than those of standard Gaussian noise. Note that this approach—reordering adversarial perturbations based on Gaussian noise ranks—is distinct from RBGM, where Gaussian noise is reordered based on adversarial perturbation ranks.

The results presented in Table 16 reveal that models trained with Gaussian noise reordering using adversarial perturbation values exhibit lower accuracy on both clean and adversarial samples compared to vanilla models. This decline in performance underscores RBGM’s ability to enhance perturbation compatibility with diffusion model training by improving statistical consistency.

Table 16: Comparison of DP_{DDPM} accuracy under different conditions and perturbation types. Training with perturbations reordered by Gaussian noise and adversarial perturbation values degrades performance.

NFEs	Clean	Vanilla		ADDT _{Gaussian reordered}		
		ℓ_∞	ℓ_2	Clean	ℓ_∞	ℓ_2
5	49.51	21.78	36.13	48.40	21.10	33.40
10	73.34	36.72	55.47	71.78	34.07	52.98
20	81.45	45.21	65.23	79.99	42.43	64.21
50	85.54	46.78	68.85	83.90	46.73	68.17
100	85.94	47.27	69.34	84.54	46.98	69.33

RBGM-mapped perturbations vs. ℓ_2 -normalized perturbations To further investigate RBGM’s effectiveness in managing adversarial perturbations, we compare:

1. **ADDT**: Trained with RBGM-mapped perturbations.
2. **ADDT $_{\ell_2}$ -normalized**: Trained with raw adversarial perturbations, scaled to match the ℓ_2 norm of standard Gaussian noise. This scaling ensures that the perturbations share the same ℓ_2 norm as those mapped by RBGM, which we refer to as ℓ_2 -normalized perturbations.

As shown in Table 17, models trained with ℓ_2 -normalized perturbations tend to perform better under ℓ_2 attacks in some scenarios (possibly because these perturbations are more similar to those generated by ℓ_2 attack during testing). ADDT generally achieves better results. This advantage is particularly pronounced under ℓ_∞ attacks and in scenarios with higher NFEs. Furthermore, as shown in Table 18, ADDT yields a lower FID value, reflecting better preservation of generative capabilities.

Table 17: Comparison of DP_{DDPM} accuracy under different perturbation conditions. Training with ADDT generally achieves better results. This advantage is particularly pronounced under ℓ_∞ attacks and in scenarios with higher NFEs.

NFEs	ADDT			ADDT $_{\ell_2}$ -normalized		
	Clean	ℓ_∞	ℓ_2	Clean	ℓ_∞	ℓ_2
5	59.96	30.27	41.99	60.40	28.47	44.58
10	78.91	43.07	62.97	79.29	41.90	63.72
20	83.89	48.44	69.82	83.59	47.85	67.68
50	85.45	50.20	69.04	84.83	49.12	69.24
100	85.64	51.46	70.12	84.97	49.95	69.29

Table 18: FID scores of DP_{DDPM} under different training conditions. Training with ADDT result in lower FID score compared to ℓ_2 normalization.

	Clean fine-tuning	ADDT	ADDT $_{\ell_2}$ -normalized
FID	3.50	5.190	5.678

As discussed in Appendix K.1, the goal of utilizing RBGM to generate perturbations is to mimic the characteristic of Gaussian noise, hence aligning ADDT closer to traditional diffusion model training. In this context, both RBGM and ℓ_2 normalization serve as approximations of Gaussian noise. Yet, RBGM provides a more precise approximation, enhancing robustness and maintaining the generative performance more effectively than ℓ_2 normalization.

L EVALUATION WITH FIXED AUTOATTACK

AutoAttack (Croce & Hein, 2020), an ensemble of White-box and Black-box attacks, is a popular benchmark for evaluating model robustness. It is used in RobustBench (Croce et al., 2020) to evaluate over 120 models. However, Nie et al. (2022) finds that the *Rand* version of AutoAttack, designed to evaluate stochastic defenses, sometimes yields higher accuracy than the *Standard* version that is intended for deterministic methods. Our comparison of AutoAttack and PGD20-EoT10 in Table 19 also shows that the *Rand* version of AutoAttack gives higher accuracy than the PGD20-EoT10 attack.

We attribute this to the sample selection of AutoAttack. As an ensemble of attack methods, AutoAttack selects the final adversarial sample from either the original input or the attack results. However, the original implementation neglects stochasticity and considers a adversarial sample to be sufficiently adversarial if it gives a false result in one evaluation. To fix this, we propose a 20-iteration evaluation and selects the adversarial example with the lowest accuracy. The flawed code is in the official GitHub main branch, git version `a39220048b3c9f2cca9a4d3a54604793c68eca7e`, and specifically in lines #125, #129, #133-136, #157, #221-225, #227-228, #231 of the file `'autoattack/autoattack.py'`. We will open source our updated code and encourage future stochastic defense methods to be evaluated against the fixed code. The code now can be found at: <https://anonymous.4open.science/r/auto-attack-595C/README.md>.

After the fix, robust accuracy under AutoAttack drops by up to 10 points, producing similar results to our PGD20-EoT10 test results. However, using AutoAttack on DP_{DDPM} with $S = 1000$ took nearly 25 hours, five times longer than PGD20-EoT10, so we will use PGD20-EoT10 for the following test.

Table 19: AutoAttack (*Rand* version) and PGD20-EoT10 performance on DBP methods for CIFAR-10 (the lower the better). The original AutoAttack produces high accuracy (%), after fixing, it achieves similar results to PGD20+EoT10 attack.

Method	l_∞			l_2		
	AutoAttack	AutoAttack _{Fixed}	PGD20-EoT10	AutoAttack	AutoAttack _{Fixed}	PGD20-EoT10
DiffPure	62.11	56.25	55.96	81.84	76.37	75.78
DP _{DDPM} -1000	57.81	46.88	48.63	71.68	71.09	72.27
DP _{DDIM} -100	50.20	40.62	44.73	77.15	70.70	71.68

Table 20: Clean and robust accuracy (%) on different DBP methods for CIFAR-10, evaluated with AutoAttack_{ADDT} (*Rand* version). All methods show consistent improvement when fine-tuned with ADDT.

Method	Vanilla			ADDT		
	Clean	l_∞	l_2	Clean	l_∞	l_2
DiffPure	89.26	56.25	76.37	89.94	58.20	77.34
DP _{DDPM}	85.94	46.88	71.09	85.64	48.63	72.27
DP _{DDIM}	88.38	40.62	70.70	88.77	44.73	71.68

M COMPARING RBGM-MAPPED PERTURBATIONS WITH l_∞ PERTURBATIONS

In Section 6.3, we briefly explore the generation capabilities of diffusion models trained with RBGM-mapped and l_∞ perturbations. Here, we provide further experiment and delve deeper into their robustness comparison. To train with l_∞ perturbations, we adjust ADDT, replacing RBGM-mapped perturbations with l_∞ perturbations. Here, instead of converting accumulated gradients to Gaussian-like perturbations, we use a 5-step projected gradient descent (PGD-5) approach. For fair comparison, we also set $\lambda_{unit} = 1$, $\lambda_{min} = 0$, $\lambda_{max} = 10$ and refer to this modified training protocol as ADDT $_{l_\infty}$.

Table 21: Clean and robust accuracy (%) on DBP models trained with different perturbations for CIFAR-10. While ADDT simultaneously improves clean accuracy and robustness against both l_2 and l_∞ attacks. ADDT $_{l_\infty}$ primarily improves performance against l_∞ attacks.

Method	Dataset	Vanilla			ADDT			ADDT $_{l_\infty}$		
		Clean	l_∞	l_2	Clean	l_∞	l_2	Clean	l_∞	l_2
DP _{DDPM} -1000	CIFAR-10	85.94	47.27	69.34	85.64	51.46	70.12	84.47	52.64	68.55
	CIFAR-100	57.52	20.41	37.89	59.18	23.73	41.70	57.81	23.24	40.04
DP _{DDIM} -100	CIFAR-10	88.38	42.19	70.02	88.77	46.48	71.19	88.48	50.49	70.31
	CIFAR-100	63.28	15.23	36.62	66.02	18.85	39.84	64.84	20.31	39.36

We evaluate the clean and robust accuracy of ADDT and ADDT $_{l_\infty}$ fine-tuned models. These models exhibit different behaviors. As shown in Table 21, while Gaussian-mapped perturbations can simultaneously improve clean accuracy and robustness against both l_2 and l_∞ attacks, training with l_∞ perturbations primarily improves performance against l_∞ attacks.

N ADDITIONAL EXPERIMENTS UNDER DETERMINISTIC WHITE-BOX SETTING

Evaluation across different models We extend our analysis to include VPSDE and EDM models under the proposed Deterministic White-Box (DW-box) attack scenario. The results, presented in Table 22, demonstrate that ADDT consistently improves robustness across different models.

Evaluation across different NFEs We also investigate the robustness under the Deterministic White-box Setting across varying NFEs. The comparison of performance between vanilla models and

Table 22: DW-box accuracy (%) under ℓ_∞ perturbations for various models. ADDT consistently improves robustness across all models.

Model	Vanilla	ADDT
DP _{DDPM}	16.80	39.16
DP _{DDIM}	4.98	17.09
DiffPure	22.76	51.63
DP _{EDM}	13.33	32.94

ADDT fine-tuned models, shown in Figure 11, highlights that ADDT consistently enhances model performance at different NFEs. This improvement is particularly pronounced at lower NFEs, further confirming that ADDT enables diffusion models to more effectively counter adversarial perturbations.

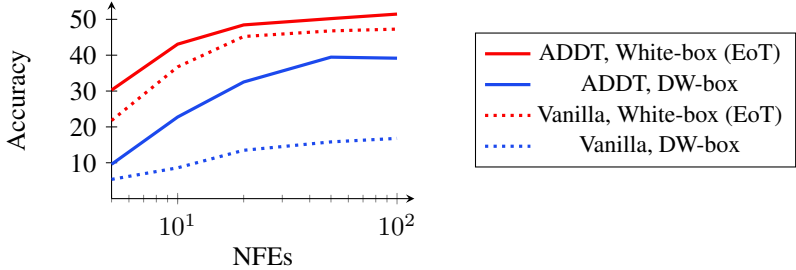


Figure 11: Revisiting Deterministic White-box Robustness. ADDT consistently improves robustness under both White-box and Deterministic White-box setting, implying that ADDT strengthens the models’ ability to handle adversarial inputs.

O SENSITIVITY ANALYSIS OF λ_{unit}

In Section 6.1 we choose $\lambda_{unit}=0.03$ because most of the adversarial perturbations are in this range. We also provide an ablation study here, which shows that the performance of ADDT is insensitive to λ_{unit} and gets a consistent improvement.

Table 23: The performance under different NFEs of ADDT training with different λ_{unit} , ADDT is insensitive to it and gets a consistent improvement on robust accuracy (%).

NFEs	ℓ_∞				ℓ_2			
	Vanilla	0.02	0.03	0.04	Vanilla	0.02	0.03	0.04
5	21.78	24.02	30.27	31.25	36.13	41.99	41.99	49.02
10	36.72	40.92	43.07	44.92	55.47	61.72	62.97	64.45
20	45.21	48.14	48.44	50.68	65.23	67.48	69.82	69.24
50	46.78	48.83	50.20	51.07	68.85	69.82	69.04	69.53
100	47.27	48.93	51.46	50.88	69.34	70.31	70.12	69.92

P COMPUTATIONAL COST ANALYSIS FOR TRAINING AND INFERENCE

Fine-tuning DDPM and DDIM models using ADDT to achieve near-optimal performance requires 50 epochs and approximately 12 hours of training on 4 NVIDIA GeForce RTX 2080 Ti GPUs. This efficiency matches that of traditional adversarial training approaches and is notably faster than recent adversarial training techniques that utilize diffusion models for dataset augmentation (Wang et al., 2023). However, testing DP_{DDPM} and DP_{DDIM} involves significant computational expense due to the use of Expectation over Transformation (EoT). For instance, validating 1,024 images on the CIFAR10/CIFAR100 datasets takes approximately 5 hours on the same GPU configuration.

One of the key advantages of ADDT is its "train-once" approach. Once the initial training is complete, ADDT can protect multiple classifiers without requiring additional fine-tuning, as demonstrated in Table 4. This is in stark contrast to adversarial classifier training, where each classifier demands individual training.

1404 During inference, models trained with ADDT have a similar complexity to standard DBP. However,
1405 their performance gains in accelerated scenarios offer the potential for a reduction in computational
1406 overhead. As shown in Table 3, $DP_{DDPM} + ADDT$ achieves comparable performance to DP_{DDPM}
1407 while requiring only 20 NFEs, resulting in up to an 80% reduction in computation time compared to
1408 the 100 NFEs required for DP_{DDPM} .
1409

1410 Q CREDIBILITY OF OUR PAPER

1411
1412 The code was developed independently by two individuals and mutually verified, with consistent
1413 results achieved through independent training and testing. We will also make the code open-source
1414 and remain committed to advancing the field.
1415

1416 R BROADER IMPACT AND LIMITATIONS

1417
1418 Our work holds significant potential for positive societal impacts across various sectors, including
1419 autonomous driving, facial recognition payment systems, and medical assistance. We are dedicated
1420 to enhancing the safety and trustworthiness of global AI applications. However, there are potential
1421 negative societal impacts, particularly concerning privacy protection, due to adversarial perturbations.
1422 Nonetheless, we believe that the positive impacts generally outweigh the potential negatives. Regarding
1423 the limitations, our approach could benefit from integrating insights from traditional adversarial
1424 training methods (Zhang et al., 2019; Shafahi et al., 2019; Wang et al., 2023), such as through more
1425 extensive data augmentation and a refined ADDT loss design. Nevertheless, these limitations are
1426 minor and do not significantly detract from the overall contributions of this paper. We believe that
1427 these new findings and perspectives could have a sustained impact on future research on DBP, which
1428 is a promising approach to adversarial defense and could be more valuable for real-world applications,
1429 although existing studies on DBP are at an early stage.
1430

1431
1432
1433
1434
1435
1436
1437
1438
1439
1440
1441
1442
1443
1444
1445
1446
1447
1448
1449
1450
1451
1452
1453
1454
1455
1456
1457